NASA/TM–2015-218998

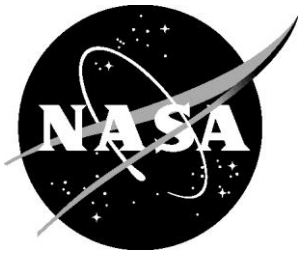

Calculated Low-Speed Steady and Time-Dependent Aerodynamic Derivatives for Some Airfoils Using a Discrete Vortex Method

Donald R. Riley
Langley Research Center, Hampton, Virginia

December 2015

NASA STI Program . . . in Profile

Since its founding, NASA has been dedicated to the advancement of aeronautics and space science. The NASA scientific and technical information (STI) program plays a key part in helping NASA maintain this important role.

The NASA STI program operates under the auspices of the Agency Chief Information Officer. It collects, organizes, provides for archiving, and disseminates NASA's STI. The NASA STI program provides access to the NTRS Registered and its public interface, the NASA Technical Reports Server, thus providing one of the largest collections of aeronautical and space science STI in the world. Results are published in both non-NASA channels and by NASA in the NASA STI Report Series, which includes the following report types:

- TECHNICAL PUBLICATION. Reports of completed research or a major significant phase of research that present the results of NASA Programs and include extensive data or theoretical analysis. Includes compilations of significant scientific and technical data and information deemed to be of continuing reference value. NASA counter-part of peer-reviewed formal professional papers but has less stringent limitations on manuscript length and extent of graphic presentations.

- TECHNICAL MEMORANDUM. Scientific and technical findings that are preliminary or of specialized interest, e.g., quick release reports, working papers, and bibliographies that contain minimal annotation. Does not contain extensive analysis.

- CONTRACTOR REPORT. Scientific and technical findings by NASA-sponsored contractors and grantees.

- CONFERENCE PUBLICATION. Collected papers from scientific and technical conferences, symposia, seminars, or other meetings sponsored or co-sponsored by NASA.

- SPECIAL PUBLICATION. Scientific, technical, or historical information from NASA programs, projects, and missions, often concerned with subjects having substantial public interest.

- TECHNICAL TRANSLATION. English-language translations of foreign scientific and technical material pertinent to NASA's mission.

Specialized services also include organizing and publishing research results, distributing specialized research announcements and feeds, providing information desk and personal search support, and enabling data exchange services.

For more information about the NASA STI program, see the following:

- Access the NASA STI program home page at http://www.sti.nasa.gov

- E-mail your question to help@sti.nasa.gov

- Phone the NASA STI Information Desk at 757-864-9658

- Write to:
  NASA STI Information Desk
  Mail Stop 148
  NASA Langley Research Center
  Hampton, VA 23681-2199

NASA/TM–2015-218998

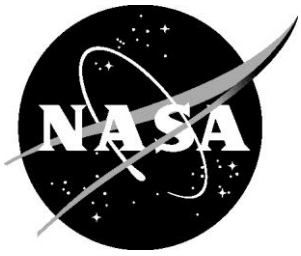

Calculated Low-Speed Steady and Time-Dependent Aerodynamic Derivatives for Some Airfoils Using a Discrete Vortex Method

Donald R. Riley
Langley Research Center, Hampton, Viriginia

National Aeronautics and
Space Administration

Langley Research Center
Hampton, Virginia 23681-2199

December 2015

Acknowledgments

The author would like to thank graphic artist G. Lee Pollard of NCI Information Systems for creating the final figures used in this report.

Available from:

NASA STI Program / Mail Stop 148
NASA Langley Research Center
Hampton, VA 23681-2199
Fax: 757-864-6500

Summary

This paper contains a collection of some results of four individual studies presenting calculated numerical values for airfoil aerodynamic stability derivatives in unseparated inviscid incompressible flow due separately to angle-of-attack, pitch rate, flap deflection, and airfoil camber using a discrete vortex method. Both steady conditions and oscillatory motion were considered. Variables include the number of vortices representing the airfoil, the pitch axis / moment center chordwise location, flap chord to airfoil chord ratio, and circular or parabolic arc camber. Comparisons with some experimental and other theoretical information are included. The calculated aerodynamic numerical results obtained using a limited number of vortices provided in each study compared favorably with thin airfoil theory predictions. Of particular interest are those aerodynamic results calculated herein (such as induced drag) that are not readily available elsewhere.

Introduction

Calculated numerical values for aerodynamic coefficients and stability derivatives for some airfoils in unseparated inviscid incompressible flow using a discrete vortex method consisting of a limited number of two-dimensional vortices were obtained for both steady conditions and sinusoidal oscillatory motion. Derivatives were calculated individually with respect to angle-of-attack, pitch rate, and flap deflection. In addition the effect of airfoil camber in steady flow was examined separately. The aerodynamic derivatives due to each of the four variables were examined in considerable detail and the information is presented here as a collection of the results of the four individual studies labeled as Section A through D in the order in which the effort was undertaken. The collection is believed to address some of the aerodynamic interest in airfoils at low speed and oscillatory frequencies relevant to vehicle dynamic stability.

A number of theoretical studies of airfoils in steady and oscillatory conditions exist in the published literature over the past 75 years (for oscillatory examples see textbooks like reference 1, numerous NACA/NASA Reports, AIAA Journal Articles, AGARD publications like reference 2, and many others). These studies examine the problem for a range of conditions including subsonic and supersonic Mach Numbers as well as for incompressible flow. Nearly all mathematical developments were restricted to the linear range of small angles and rates and address the airfoil flow condition at the trailing edge (the Kutta condition). The discrete vortex method circumvents the Kutta condition by substituting a boundary condition at the three-quarter-chord location that yields equivalent aerodynamic results. The purpose of this effort, which was part of a larger exploratory investigation including both airfoils and wings, was to apply the discrete vortex method to assess the use of a limited number of vortices to yield realistic values of the aerodynamic derivatives.

Symbols*

A	amplitude
c	airfoil chord, *ft.*
c_f	flap chord, *ft.*
c_d	section drag coefficient, $d / .5\rho V^2 c$
c_h	section flap hinge-moment coefficient, $h / .5\rho V^2 \left(c_f\right)^2$
c_ℓ	flap lift coefficient, $\ell / .5\rho V^2 c$
c_l	section lift coefficient, $l / .5\rho V^2 c$
c_m	section pitching-moment coefficient, $m / .5\rho V^2 c^2$
c_p	pressure coefficient, $\Delta p / .5\rho V^2$
d	airfoil drag force, *lbs. per unit span*
h	flap hinge-moment, *ft.-lbs. per unit span*
k	reduced frequency parameter, ω*c/2V*
K_n	individual vortex circulation value, *ft^2 / sec.*
ℓ	flap lift, *lbs. per unit span*
l	airfoil lift force, *lbs. per unit span*
m	airfoil section pitching moment, *ft.-lbs. per unit span*
N	number of vortices used
ρ	mass density of air, $slugs / ft^3$
V	velocity, *ft./sec*
t	time, *sec.*
z	camber parameter, $\frac{a}{c}$ (circle) or $\frac{y_e}{c}$ (parabola)
α	airfoil angle of attack, *radians*
q	airfoil pitch-rate, *radians per sec.*
δ	flap deflection, *radians*
α_f	flap angle of attack, *radians*
q_f	flap pitch-rate about flap leading edge, *radians per sec.*
ω	circular angular velocity, *radians/sec.*
θ	pitch angle, *radians*
Φ	indicial function
ϕ	slope of the mean line, r*adians*
ϕ_e	trailing edge angle, *radians*

$$c_{b_\alpha} = \frac{\partial c_b}{\partial \alpha} \qquad c_{b_{\dot\alpha}} = \frac{\partial c_b}{\partial \frac{\dot\alpha c}{2V}} \qquad c_{b_q} = \frac{\partial c_b}{\partial \frac{qc}{2V}} \qquad c_{b_{\dot q}} = \frac{\partial c_b}{\partial \frac{\dot q c^2}{[2V]^2}}$$

$$c_{b_{\alpha f}} = \frac{\partial c_b}{\partial \alpha f} \qquad c_{b_{\dot\alpha f}} = \frac{\partial c_b}{\partial \frac{\dot\alpha fc}{2V}} \qquad c_{b_{qf}} = \frac{\partial c_b}{\partial \frac{qfc}{2V}} \qquad c_{b_{\dot q f}} = \frac{\partial c_b}{\partial \frac{\dot q fc^2}{[2V]^2}}$$

$$c_{b_\delta} = \frac{\partial c_b}{\partial \delta}$$

Oscillating Conditions:

$$c_{b_\delta} = c_{b_{\alpha f}} - k^2 c_{b_{\dot q f}} \qquad c_{b_{\dot\delta}} = c_{b_{qf}} + c_{b_{\dot\alpha f}}$$

where $b = l., \ell, h, m$

Subscripts:

0	amplitude of sinusoidal motion
α	due to angle of attack
q	due to pitch rate
ss	steady state

*A dot over a symbol represents a derivative with respect to time.

Theory

A thin symmetrical airfoil is chosen to be represented by its chord that is divided into a number of segments. A vortex is located at the one-quarter position of each segment and a control point at the three-quarter position. The velocity generated by the sum of all vortices at each control point is set equal to the external wind velocity normal to the airfoil surface. Solution of the set of simultaneous equations yields values for the unknown circulations and thus the lift for steady conditions. For time-dependent calculations use is made of starting vortices positioned at a quarter-chord aft of the trailing edge at time equals zero. As time increases vortices are shed downstream in the wake. Calculation of the lift on the airfoil surface at each new wake location yields the response to a step-input. From this indicial function, additional calculations can provide the frequency response from which the aerodynamic derivatives as a function of reduced frequency, k, can be obtained. Calculations are made separately for angle-of-attack and pitch-rate, and when summed the result corresponds to wind-tunnel sinusoidal oscillatory measurements (see Appendix A).

Presentation Of Results

The four individual studies are identified briefly as follows:

Section A – Steady aerodynamic derivatives for angle of attack and pitch rate

Section B – Oscillatory aerodynamic derivatives for angle-of-attack and pitch rate

Section C – Steady and oscillatory aerodynamic derivatives due to flap deflection

Section D –Steady aerodynamics due to circular and parabolic arc camber

Results and Discussion

The calculated aerodynamic results presented in each section compared favorably with thin airfoil theory predictions. Of particular interest are those aerodynamic results calculated herein that are not readily available elsewhere. These are worth noting and include: (1) the load distribution across the chord for steady pitch rate, (2) values for the induced drag coefficient for oscillatory motion, (3) airfoil and flap motions that result in lift and pitching moment versus displacement traces having unusual shapes, and (4) slight differences in the aerodynamics between circular and parabolic arc camber.

Section A - Steady aerodynamic derivatives for angle of attack and pitch rate

Consider the airfoil section to be symmetrical and thus represented by its chord. Calculated values for the angle-of-attack and pitch-rate derivatives for different numbers of vortices equally spaced across the chord are tabulated respectively in Tables 1 and 2 for five different pitch-axis/moment-center locations on the chord. The values are exact and presented in the form of fractions as calculated. Thin airfoil theory values (first given in 1928 by Glauert in reference 3 and converted here to NASA nomenclature) are also included for comparison and plotted in figure 1 to illustrate the parabolic curve for pitch damping derivative c_{m_q}. Calculated values herein for c_{l_α}, c_{m_α}, and c_{l_q} are independent of the number of vortices employed and identical to those of thin airfoil theory on figure 1. Values for c_{m_q} however approach thin airfoil values when a reasonable number of vortices are used to represent the airfoil as illustrated by figures 2 and 3. Figures 4, 5, and 6 are provided to indicate the load distribution across the airfoil chord due to angle of attack and due to pitch rate. Of particular interest is the zero value of the moment derivative due to pitch rate at the mid-chord position resulting from the up-loading on the front as well as the rear portions of the airfoil. Finally, airfoil induced drag predicted by the interaction of the various vortices for both angle–of-attack and pitch-rate conditions was found to be zero as expected and is illustrated in the example on figure 7 (for additional comments on drag see Appendix B).

Table 1. - Aerodynamic Derivatives Due to Angle of Attack

Number of Vortices	Moment Center Chordwise Location										
	Leading Edge		**Quarter Chord**		**Mid Chord**		**Three-Quarter Chord**		**Trailing Edge**	
	c_{l_α}	c_{m_α}	c_{l_α}	c_{m_α}	c_{l_α}	c_{m_α}	c_{l_α}	c_{m_α}	c_{l_α}	c_{m_α}
	Mathematical Exact Value									
1	2π	$-\frac{1}{2}\pi$	2π	0	2π	$+\frac{1}{2}\pi$	2π	$+1\pi$	2π	$+\frac{3}{2}\pi$
2	2π	$-\frac{1}{2}\pi$	2π	0	2π	$+\frac{1}{2}\pi$	2π	$+1\pi$	2π	$+\frac{3}{2}\pi$
3	2π	$-\frac{1}{2}\pi$	2π	0	2π	$+\frac{1}{2}\pi$	2π	$+1\pi$	2π	$+\frac{3}{2}\pi$
4	2π	$-\frac{1}{2}\pi$	2π	0	2π	$+\frac{1}{2}\pi$	2π	$+1\pi$	2π	$+\frac{3}{2}\pi$
∞ *	2π	$-\frac{1}{2}\pi$	2π	0	2π	$+\frac{1}{2}\pi$	2π	$+1\pi$	2π	$+\frac{3}{2}\pi$
	Computer Calculated Values									
8	2π	$-.5000\pi$	2π	0	2π	$.5000\pi$	2π	1.0000π	2π	$+1.5000\pi$

* Thin airfoil theory values

Table 2. - Aerodynamic Derivatives Due to Pitch Rate

Number of Vortices	Pitch-Axis / Moment-Center Chordwise Location									
	Leading Edge		**Quarter Chord**		**Mid Chord**		**Three-Quarter Chord**		**Trailing Edge**	
	c_{l_q}	c_{m_q}	c_{l_q}	c_{m_q}	c_{l_q}	c_{m_q}	c_{l_q}	c_{m_q}	c_{l_q}	c_{m_q}
	Mathematical Exact Value									
1	3π	$-\frac{3}{4}\pi$	2π	0	π	$+\frac{1}{4}\pi$	0	0	$-\pi$	$-\frac{3}{4}\pi$
2	3π	$-\frac{15}{16}\pi$	2π	$-\frac{3}{16}\pi$	π	$+\frac{1}{16}\pi$	0	$-\frac{3}{16}\pi$	$-\pi$	$-\frac{15}{16}\pi$
3	3π	$-\frac{35}{36}\pi$	2π	$-\frac{8}{36}\pi$	π	$+\frac{1}{36}\pi$	0	$-\frac{8}{36}\pi$	$-\pi$	$-\frac{35}{36}\pi$
4	3π	$-\frac{63}{64}\pi$	2π	$-\frac{15}{64}\pi$	π	$+\frac{1}{64}\pi$	0	$-\frac{15}{64}\pi$	$-\pi$	$-\frac{63}{64}\pi$
∞ *	3π	$-\pi$	2π	$-\frac{1}{4}\pi$	π	0	0	$-\frac{1}{4}\pi$	$-\pi$	$-\pi$
	Computer Calculated Values									
8	3π	$-.9961\pi$	2π	$-.2461\pi$	π	$.0039\pi$	0	$-.2461\pi$	$-\pi$	$-.9961\pi$

* Thin airfoil theory values

Section B - Oscillatory aerodynamic derivatives for angle of attack and pitch rate

Consider the airfoil to be symmetrical and thus represented by its chord. Calculations were made considering the airfoil to be in rectilinear motion at time equals zero and then a step input is applied in angle of attack and separately in pitch rate. A starting vortex is positioned at c/4 aft of the airfoil trailing edge at t=0 that moves downstream with increasing time. Figures 8 and 9 illustrate the vortex arrangements that were used in the calculations for the wake at various positions downstream. The resulting indicial function developed was then used to determine the frequency response. As in the case for steady motion, calculations were made for five pitch-axis locations equally spaced across the chord from the leading edge to the trailing edge. Figures 10 and 11 give the lift and pitching moment results for a step input in angle of attack as a function of downstream location. Figure 12 gives the corresponding induced drag function resulting from the interaction of the vortices in the wake with those on the airfoil. The equation on figure 12, although not an indicial function, can be used to estimate the induced drag coefficient with wake positions further downstream. An examination of the figure shows the maximum induced drag value occurs just before the wake has proceeded one chord length downstream. As time increases and the wake continues to move downstream the induced drag force decreases until the steady-state condition is reached at which time the induced drag is zero.

Using the indicial functions developed from figures 10 and 11, calculations were made to obtain the corresponding lift and pitching-moment frequency response results. Figures 13 and 14 give the lift and pitching-moment derivatives c_{l_α}, $c_{l_{\dot\alpha}}$, c_{m_α}, and $c_{m_{\dot\alpha}}$ as a function of reduced frequency parameter k. Figures 15 and 16 are included here to illustrate the use of figures 13 and 14 to obtain typical responses to sinusoidal plunging oscillations of a thin two-dimensional airfoil. These figures show lift-displacement and moment-displacement traces for a given value of reduced frequency. In the case of the induced drag, figure 12 shows $E_{d\alpha}$ is not an indicial function, however the square root of $E_{d\alpha}$ labeled $\Phi_{d\alpha}$ in figure 17 can be considered as such. Frequency response results permit establishing a sinusoidal time history trace of the $\sqrt{c_d}$ function. Squaring this result provides a time history of the induced drag parameter that is twice the motion frequency and from which the induced-drag—displacement trace can be constructed. Note that to obtain a drag comparison with experimental data, the profile drag contribution must be added to the induced drag component shown.

Calculated results for the lift, pitching moment, and induced drag due to a step input in pitch rate were also determined. From this information, frequency response results for the lift and pitching moment derivatives shown on figures 18 and 19 were obtained as a function of reduced frequency parameter k. Step-response results obtained for the induced drag function due to pitch rate are given in figure 20 for completeness, however further effort with this induced drag information was not undertaken.

Combination derivatives representative of low-speed wind-tunnel aerodynamic measurements of an airfoil pitching about a point on the airfoil chord were obtained by appropriately summing the angle-of-attack and pitch-rate derivatives. Figures 21 and 22 provide these derivative values for the five different pitch-axis/moment-center locations on

the chord. An examination of the numerical results in general show a reduction in the derivative magnitude with an increase in oscillation frequency.

Some comparisons of values from calculations made herein using 4 vortices to represent the airfoil with other theoretical values and experimental measurements are presented in figures 23 thru 27. Figures 23 and 24 give comparisons of the airfoil indicial-lift function with Wagner's prediction and figure 24 with Theodorsen's prediction. (See reference 5.) Comparison of the combined derivative values calculated herein with wind-tunnel measurements given by Halfman in reference 4 converted to the nomenclature of this paper and adjusted by the inverse of the experimental measured lift-curve-slope ratio $\frac{c_{l_\alpha}}{2\pi}$ of 0.813 for steady conditions is given in figures 25, 26 and 27. The experiment was conducted on a 1-foot chord, 2-foot span NACA 0012 airfoil mounted between two large vertical fairings in the 5- by 7- foot test section of the Massachusetts Institute of Technology flutter tunnel. The supporting mechanism could provide sinusoidal oscillatory vertical motion (± 1 inch and ± 2 inches) and angular rotations about the 37% chord position either independently or in combination for a reduced frequency range for k from about .05 to about .45. Considering the differences existing between the mathematical models and the wind-tunnel experimental set-up, the data comparisons shown in the figures appear reasonable.

Section C - Steady and oscillatory aerodynamic derivatives due to flap deflection

The airfoil is considered symmetrical so that it can be represented by its chord. The chord is divided into a number of segments according to the number of vortices chosen to represent the airfoil. Vortices and control points were positioned on the chord line according to the one-quarter---three-quarter rule for each segment. The hinge line for flap deflection was placed at a segment leading edge. This arrangement corresponds to a plain flap with gap sealed. Calculations for selected values of the ratio of flap chord to airfoil chord were chosen to cover the range from 0 to1. All angle and rates are assumed small. Steady conditions are considered first followed by oscillatory motion.

Calculated values for the airfoil aerodynamic derivatives c_{l_δ} and c_{m_δ} using different numbers of vortices representing the airfoil are given in figure 28. The ordinate $\frac{c_{l_\delta}}{2\pi}$ on figure 28 also can be interpreted as $\frac{\Delta\alpha}{\Delta\delta}$. As a consequence the total lift coefficient with flap deflected can be written as $c_l = c_{l_\alpha}\left[\alpha + \frac{\Delta\alpha}{\Delta\delta}\delta\right]$ since the method of superposition applies. Calculated values for steady conditions of lift derivatives for the airfoil and separately for the portion of the lift derivative carried on the flap due to angle of attack is given in figure 29a. Shown on figure 29b are the corresponding lift derivatives due only to flap deflection. Some interesting comparisons can be observed from an examination of the values in the two figures. For example, consider the derivative values for $\frac{c_f}{c} = \frac{1}{2}$. For the

flap deflected (fig. 29b), 50% more lift is produced on the flap compared to the lift when the flap is in the undeflected condition (fig 29a). Lastly, deflecting the half-chord flap produces 80% of the lift produced by deflecting the complete airfoil the same amount. Calculation of the hinge-moment derivatives, c_{h_α} and c_{h_δ} were made using 8 vortices representing the airfoil and the results are given in figure 30. Derivative values were obtained for selected values of the ratio of flap chord to airfoil chord. The total hinge-moment coefficient can be written as

$$c_h = c_{h_\alpha}\alpha + c_{h_\delta}\delta$$

Also shown on figure 30 for comparison purposes are values obtained from reference 5.

For oscillatory motion, calculation of the aerodynamic response due to a step input in flap deflection (indicial response) is similar to that used to obtain the response for the airfoil in Section B. A starting vortex is located at a distance $c/4$ aft of the trailing edge and consists of all vortices used to define the airfoil with deflected flap. As the wake moves downstream with increasing time, additional vortices are inserted on the airfoil and in the wake to satisfy the boundary conditions. Aerodynamic calculations are carried out separately for a step input in flap attitude (flap angle of attack, α_f) and separately in flap angular velocity (flap pitch-rate, q_f). Figures 31, 32, 33, 34, 35, 36, and 37 are presented giving some aerodynamic derivatives for the starting condition $\frac{Vt}{c/2} = 0$ and the steady state condition $\frac{Vt}{c/2} = \infty$. The difference in the curves is an indication of the time dependency involved.

Once the indicial functions are determined the frequency response can be obtained. Figures 38 and 39 give the lift derivatives as a function of reduced frequency parameter k for two flap sizes. The figures give a comparison of the flap data with that of the complete airfoil both oscillating at the same frequency. It is interesting to note that the derivative values for the half-chord flap oscillating are about three-quarters of those for the complete airfoil oscillating.

Since the method of superposition holds for combining the lift and moment aerodynamic derivatives due individually to the α and q motions to yield values for sinusoidal oscillations, superposition can be applied to different combinations of amplitude and frequency of airfoil and flap motion. Figures 40, 41, 42, and 43 give several example lift-displacement traces that were calculated. Reference 6 presents a number of comparisons of airfoil and flap data from wind tunnel measurements with a different analytical computation showing loops like those on figures 41 and 42.

Section D - Steady aerodynamics for circular and parabolic arc camber

A limited number of calculations using a discrete vortex method in steady inviscid incompressible flow were made to obtain the effect of camber on the lift and pitching

moment of a two dimensional airfoil represented by its mean-line. Calculations were made for circular arc camber and also for parabolic arc camber. The latter camber was undertaken since NACA Four–Digit Airfoils use mean lines consisting of parabolic arcs thus permitting comparison of calculated and experimental results. Maximum camber values of 1, 2, and 4 percent of the chord along with maximum camber locations of 40, 50, and 60 percent of the chord were considered. The geometry involved and calculated values of lift and pitching moment are given and discussed. To permit calculation for different chordwise locations of maximum camber, the airfoil mean line is divided into two parts at the point of maximum camber. Each part is then divided into a number of segments with a vortex and control point assigned to each segment. For each segment, the one-quarter—three-quarter rule is applied. Since displacement of the mean line from the chord line is small for small camber, the vortices and control points are placed on the airfoil chord instead of the curved mean line to simplify the geometry involved. However, the external velocity at each control point to be canceled by the vortex system is that at the mean line since that is the local angle of attack of the surface at that point. The external velocity at each control point can be expressed in terms of the trailing edge angle ϕ_e. Solution of the matrix equation yields values of the unknown circulations as a function of the trailing edge angle ϕ_e. Using the relation between trailing edge angle ϕ_e and camber parameter z along with the Kutta-Joukowski equation gives the lift and pitching moment coefficients as a function of z where z is the maximum displacement of the mean line from the chord line in fractions of the chord. Note that for these calculations, the airfoil chord line must remain aligned with the relative wind (i.e., airfoil angle of attack remains zero). Three factors of interest in the use of camber are:

1) the amount of camber
2) the chordwise location of the maximum camber point
3) the maximum airfoil thickness

Other influences such as the equation of the camber line, Reynolds Number, Mach Number, etc., are also of concern but the three main factors were important enough that the NACA Four-Digit Airfoil Series identifies them in the airfoil designation. For example the NACA 2412 section specifies the airfoil has 2% camber (i.e., the maximum displacement of the mean line from the chord line expressed in fractions of the chord), the maximum displacement is at 40% of the chord from the leading edge, and the 12 represents the maximum thickness in percent of the chord (for additional background discussion on Camber see Appendix C).

Calculations using the geometry given in figure 44 were made to obtain the lift and pitching moment coefficients due to circular arc camber with the maximum camber point at the 50% chord location. Calculations were made using 2 and 4 vortices to represent the airfoil. Table 3 lists the calculated aerodynamic coefficients in terms of the trailing edge angle ϕ_e and also in terms of the camber parameter z.

Table 3 – Aerodynamic Coefficients For Max-Camber At Mid- Chord

Number Of Vortices	Max Camber Location	c_l	$c_{m_{c/2}}$	$c_{m_{c/4}}$
2	.50 c	$\pi\phi_e$	$\frac{1}{16}\pi\phi_e$	$-\frac{3}{16}\pi\phi_e$
4	.50 c	$\pi\phi_e$	$\frac{1}{4}(\frac{1}{16}\pi\phi_e)$	$-\frac{15}{64}\pi\phi_e$
2	.50 c	$4\pi z$	$\frac{1}{4}\pi z$	$-\frac{3}{4}\pi z$
4	.50 c	$4\pi z$	$\frac{1}{16}\pi z$	$-\frac{15}{16}\pi z$
∞	.50 c	$4\pi z$	0	$-\pi z$

Note that the table indicates that the value of lift coefficient is independent of the number of vortices used to represent the airfoil.. The value of the pitching moment coefficient, however, depends on the number of vortices representing the airfoil. The table also lists the limiting values. The zero value of the moment at the mid-chord location indicates this is the position of the center of pressure. McCormick in Reference 7 presents results using a large number of vortices illustrating the limiting value about the mid-chord is zero. The procedure used for the calculations herein is similar to that of Reference 7 with similar results. Differences, however, exist in the development of the camber geometry presented in figure 44c.

To illustrate the influence of altering the chordwise location of maximum camber, some additional calculations were made for maximum camber at the 40% and 60% chord location. For each condition, two circular arcs of different radius were chosen such that they were tangent at the point of maximum camber and that the airfoil chord was aligned with the relative wind. Figure 45 and 46 give the geometry used. Calculations were made using 2, 4, and 8 vortices representing the airfoil and the results are given in Table 4.

Table 4 – Aerodynamic Coefficients For Max-Camber At Different Chord Positions

Number of Vortices	Maximum Camber Location	c_l	$c_{m_{C/4}}$
2	.36c	.8771 (4πz)	-.5658(πz)
2	.40c	.9091 (4πz)	-.6236(πz)
2	.44c	.9434 (4πz)	-.6651(πz)
2	.50c	1.0000 (4πz)	-.7500(πz)
2	.56c	1.0638 (4πz)	-.8457(πz)
2	.60c	1.1111 (4πz)	-.9167(πz)
4	.40c	.9068 (4πz)	-.7888(πz)
4	.50c	1.0000 (4πz)	-.9375(πz)
4	.60c	1.1236 (4πz)	-1.1221(πz)
8	.40c	.9063 (4πz)	-.8316(πz)
8	.50c	1.0000 (4πz)	-.9837(πz)
8	.60c	1.1286 (4πz)	-1.1744(πz)
∞	.40c	.9063 (4πz)	-.8479(πz)*
∞	.50c	1.0000 (4πz)	-1.0000(πz)
∞	.60c	1.1286 (4πz)	-1.1907(πz)*

* Estimated using increment at mid chord

For these calculations the numerical values were expressed in digital form using eight decimal places. An examination of the tabulated values indicates both the effect of camber location and the number of vortices used. A graphic illustration is given in figure 47 and sketches of the chordwise load distributions are given in figure 48. Comparison of the ordinate numerical values of figure 48 cannot be made because the value of ϕ_e is different for the three distributions, however the shift in loading is apparent with maximum camber location. An examination of figure 47 indicates that shifting the maximum camber location forward of the mid-chord decreases the lift and adds a pitch-up increment to the moment for a given vortex representation. Shifting the maximum camber point rearward of the mid-chord gives the opposite aerodynamic result for a given vortex representation. As indicated previously in the text, the lift coefficient was found to be independent of the number of vortices employed. This fact is also shown on figure 47. Of more significance however, was the large effect on the pitching moment of increasing the number of vortices used for the calculations. Increasing the number of vortices representing the airfoil added an increment to the pitch down moment. The values for the 50% maximum camber location indicated using 8 vortices provided a numerical value of the pitching moment coefficient within 2% of that using an infinite number of vortices.

The camber geometry involved for NACA Four-Digit Airfoils is illustrated in figure 49 and consists of two parabolic curves, one curve on each side of the maximum camber

position. (See reference 8.) Recall that a parabolic curve is the locus of points equidistant from a line called the directrix and a point called the focus. The equation for the curve was obtained from reference 10. Note that the origin of the axis system is midway between the directrix and the focus. The discrete vortex method places the vortices and control points representing the airfoil on the chord to simplify the geometry involved, however the flow velocity to be cancelled by the vortex system is that on the curved surface. Calculations were made for 2, 4, and 8 vortices for maximum camber at the mid chord. The numerical results obtained were the same as those obtained for circular arc camber. In addition calculations were made for maximum camber at 40% and 60% chord locations. Since reference 9 provides experimental measurements for maximum camber at the 40% chord location, a comparison of computed values for 2% and 4% camber with values from reference 9 is given in the following Tables.

Table 5 – Comparison Of Calculated Values And Experimental Measurements

Vortex Calculated 2%Camber

Number Of Vortices	c_l	$c_{m_{c/4}}$
8	0.2278	-0.05225
∞	0.2278	-0.05328

Reference 9 Experimental Values

Airfoil Section	c_l	$c_{m_{c/4}}$
NACA 2408	0.195	-0.038
NACA 2410	0.20	-0.050
NACA 2412	0.23	-0.035

Vortex Calculated 4% Camber

Number Of Vortices	c_l	$c_{m_{c/4}}$
8	0.4556	-0.10450
∞	0.4556	-0.10655

Reference 9 Experimental Values

Airfoil Section	c_l	$c_{m_{c/4}}$
NACA 4412	0.39	-0.095

The comparison of calculated and experimental values for the 2% camber information seem reasonable for the thickness ratios presented considering the difficulty of establishing the numerical values from the figures of reference 9. For the 4% camber information it appears that the calculated values overestimate the magnitude of the lift and pitch-down moment.

The original camber derivation developed previously gave identical expressions for the aerodynamic lift and pitching moment coefficients for circular arc and parabolic arc camber. Since exact solutions would be expected to show some difference, the camber derivations were re-examined and an alternate procedure was developed for circular arc camber. Note that the origin of the axis system for the parabolic camber derivation on figure

49 was chosen to be at the vertex of the parabola on the Y-axis. For a similar situation to exist for circular arc camber the origin of the axis system must be moved from the center of the circle to a position a radial distance along the positive Y-axis. Using this set-up different relationships can be developed for parameter z and the trailing–edge angle ϕ_e as shown in Appendix D. Using this new equation for circular arc camber, the new equations for lift and pitching moment coefficients are:

$$c_l = 4\pi z\left(1 + 4z^2\right) \qquad c_{m_{c/4}} = -\pi z(1 + 4z^2)$$

The factor $\left(1 + 4z^2\right)$ indicates that for 2% camber, the increase in the aerodynamic coefficients is of the order of one-sixth of one percent of the original value. This small amount is the difference in the aerodynamic results between airfoils using circular arc and parabolic arc camber.

Concluding Remarks

Aerodynamic coefficients and stability derivatives for airfoils in unseparated inviscid incompressible flow were calculated using a discrete vortex method involving a limited number of two-dimensional vortices for both steady conditions and sinusoidal oscillatory motions at low speed and low frequencies. Comparison of calculated values for both steady state and oscillatory conditions were in fairly good agreement with those of thin airfoil theory. Limited comparisons of calculated numerical values herein with available wind-tunnel experimental measurements were considered reasonable. For oscillatory conditions induced drag values were calculated due to the interaction of the shed vortices in the wake with the vortices on the airfoil surface. For the steady condition induced drag is, of course, zero. Values of steady-state derivatives due to flap deflection were found to be in good agreement with previous published results. Aerodynamic lift for some different combinations of sinusoidal oscillatory motion of the airfoil and flap produced loops in the lift-displacement traces similar to those observed experimentally. Finally in steady flow, only very small differences were found to exist in the calculated aerodynamic results between airfoil mean-lines having circular or parabolic arc camber for small camber values. The position of the maximum camber point on the chord was found to have a significance influence on the values of the lift and pitching-moment coefficients. Comparison of calculated lift and moment magnitudes were found to overestimate somewhat the few experimental wind-tunnel measurements available.

References

1) Bisplinghoff, Raymond L. ; Ashley, Holt. ; Halfman, Robert L. : Aeroelasticity; Addison-Wesley Publishing Company Inc. 1955
2) Special Course on Unsteady Aerodynamics ; AGARD REPORT 679 March 1980
3) Glauert, H.: The Lift and Pitching Moment of an Airfoil Due to a Uniform Angular Velocity in Pitch R. & M. No. 1216, British A.R.C., 1928
4) Halfman, Robert L. : Experimental Aerodynamic Derivatives of a Sinusoidally Oscillating Airfoil in Two-Dimensional Flow NACA TR 1108 1952
5) Etkin. Bernard : Dynamics of Atmospheric Flight ; John Wiley and Sons, Inc. c 1972
6) Krzysiak, A. and Narkiewicz, J. : Aerodynamic Loads On Airfoil With Trailing-Edge Flap Pitching With Different Frequencies ; AIAA Journal Of Aircraft , March-April 2006
7) McCormick, Barnes W. : Aerodynamics, Aeronautics, and Flight Mechanics ; John Wiley & Sons, Inc. 1979
8) Wood, Karl D.: Technical Aerodynamics; McGraw-Hill Book Company Inc. 1947
9) Abbott, Ira H. and Von Doenhoff, Albert E. : Theory of Wing Sections (including a summary of airfoil data) Dover Publications Inc. New York 1959
10) James/ James : Mathematics Dictionary : Fourth Edition ; Van Nostrand Rienhold Company; New York. NY 1976
11) Von Karman, Theodore : AERODYNAMICS Selected Topics in the Light of Their Historical Development Dover Publications, Inc. 2004
12) Vincenti, Walter G. : What Engineers Know And How They Know It (analytical studies from aeronautical history) The John Hopkins University Press, 1990
13) Hanson, James B. : Engineer In Charge (A History of the Langley Aeronautical Laboratory 1917 – 1958) The NASA Historical Series NASA SP4305; 1987

Appendix A – Wind-Tunnel Measurements

Consider a thin two-dimensional airfoil performing sinusoidal oscillations in pitch about an axis on the airfoil chord. Assume the air-stream is horizontal and in a direction parallel to the wind-tunnel centerline. If θ designates the pitch angle of the airfoil relative to the wind-tunnel centerline, then the following expressions apply:

$$\theta = \theta_0 \sin \omega t$$
$$\dot{\theta} = \theta_0 \omega \cos \omega t$$
$$\ddot{\theta} = -\theta_0 \omega^2 \sin \omega t$$

where θ is the instantaneous pitch angle of the airfoil at any time t and θ_0 is the amplitude of the motion. The aerodynamic lift coefficient due to the oscillatory motion can be written as:

$$C_l = C_{l\alpha}\,\alpha + C_{l\,\dot{\alpha}}\,\frac{\dot{\alpha}c}{2V} + C_{lq}\,\frac{qc}{2V} + C_{l\dot{q}}\,\frac{\dot{q}}{4}\left(\frac{c}{V}\right)^2$$

Recognizing that

$$\alpha = \theta \qquad q = \dot{\theta}$$
$$\dot{\alpha} = \dot{\theta} \qquad \dot{q} = \ddot{\theta}$$

Then upon proper substitution gives

$$C_l = C_{l\alpha}\,\theta_0 \sin \omega t + C_{l\,\dot{\alpha}}\,\theta_0\,\frac{\omega c}{2V}\cos \omega t + C_{lq}\,\theta_0\,\frac{\omega c}{2V}\cos \omega t - C_{l\dot{q}}\,\theta_0\left(\frac{\omega c}{2V}\right)^2 \sin \omega t$$

Collecting similar terms and letting $k = \frac{\omega c}{2V}$ gives:

$$C_l = \left(C_{l\alpha} - k^2 C_{l\dot{q}}\right)\theta_0 \sin \omega t + \left(C_{lq} + C_{l\,\dot{\alpha}}\right) k\,\theta_0 \cos \omega t$$

Each term of this equation is a function of the motion amplitude and each is a function of reduced frequency. The first term is in-phase with the airfoil angular displacement θ and the second term is out-of-phase with θ. An analogous development can be made for the pitching moment yielding:

$$C_m = \left(C_{m\alpha} - k^2 C_{m\dot{q}}\right)\theta_0 \sin \omega t + \left(C_{m_q} + C_{m\,\dot{\alpha}}\right) k\theta_0 \cos \omega t$$

An equation for drag coefficient similar to the lift and moment equations given above cannot be written since the induced drag is a nonlinear function of the α and q variables.

Appendix B – Comment On Airfoil Drag At Steady Flow Conditions

It is interesting to observe that Jean Le Rond d'Alembert (a famous French mathematician born in 1717 and died in 1783) examined the airfoil drag problem for steady unseparated inviscid incompressible (potential) flow. The inviscid flow assumption specified that the friction drag component is zero. Potential flow specified that the flow leaves smoothly from the trailing edge along a streamline (the Kutta condition). Thus no separation and no discontinuities exist at the trailing edge. As a consequence, full pressure recovery occurs on the rear of the airfoil and thus pressure drag is zero. Since profile drag is the sum of the friction drag and pressure drag components, it is also zero. The remaining drag component that can exist is that of induced drag and it also is found to be zero. Thus occurs d'Alembert's paradox—the two dimensional airfoil at an angle of attack produces a lift force but pays no penalty since drag is zero which is a quite unusual and unexpected result. d'Alembert worked to obtain a drag force rather than this unusual result for a number of years without success. Von Karman in reference 11 indicates zero drag is the correct result and it is the result given by the discrete vortex method.

Appendix C - Background Discussion on Airfoil Camber

Low speed aerodynamic characteristics for wings and airfoils are divided into planform effects and section effects. Planform effects involve variations in shape, aspect ratio, taper ratio, sweep angle, etc. The first useful developed wing theory was Prandtl's lifting-line theory followed much later by vortex lattice and lifting surface schemes among others. Section effects were addressed by Max Munk (references 12 and 13) and others in the early 1920's and resulted in the well known "thin airfoil theory". In this theory the airfoil section is represented by its mean line that is the line from the leading edge to the trailing edge half way between the upper and lower airfoil surfaces. Lift and pitching moment are associated with the shape of this line. Thickness distribution about the mean line provides the section shape and is responsible along with skin friction for the airfoil drag force. If the airfoil has a symmetrical section then the mean line is the chord line. For this situation the aerodynamic center is located at the one-quarter chord location, the lift curve slope is 2π, and the pitching moment coefficient is zero. For the mean line displaced from the chord line both lift and pitching moment are obtained. Curvature of the mean line is usually designated by an equation and denoted by the maximum vertical displacement from the chord and its chordwise station aft of the leading edge. For airfoil section lift and pitching moment, angle of attack and curvature effects are additive for steady conditions. Because of the presence of the boundary layer, some difference exists between theory and experiment. Section drag is usually obtained experimentally. Over the years a large number of airfoil sections have been designed and tested experimentally in wind tunnels. A collection of some of this information is given in a book entitled *Theory of Wing Sections* by Abbott and Von Doenhoff (ref. 9).

Appendix D - Alternate Circular-Arc Camber Derivation (max camber at 50% chord)

The origin of the axis system for the parabolic camber derivation (figure 49) was chosen to be at the vertex of the parabola on the Y-axis. For a similar situation to exist for circular arc camber, the origin of the axis system must be moved from the center of the circle to a position a radial distance along the positive Y-axis. Using this set-up,

relationships can be developed between the camber parameter z and the trailing-edge angle ϕ_e. The equation for a circle with the axis system origin at the center of the circle is:

$$x^2 + y^2 = R^2$$

The equation of a circle with the axis-system origin displaced vertically with the X-axis tangent to the circle is:

$$x^2 + \left(y' + R\right)^2 = R^2$$
$$x^2 + y'^2 + 2Ry' + R^2 = R^2$$
$$x^2 + y'^2 = -2Ry'$$

Taking the derivative

$$2xdx + 2y'dy' = -2Rdy'$$
$$xdx + y'dy' = -Rdy'$$
$$xdx = -\left(y' + R\right)dy'$$
$$\frac{dy'}{dx} = -\frac{x}{y' + R}$$

Replacing R gives

$$\frac{dy'}{dx} = \frac{-x}{y' + \left(\frac{x^2 + y'^2}{-2y'}\right)} = \frac{x2y'}{-2y'^2 + x^2 + y'^2} = \frac{2xy'}{x^2 - y'^2}$$

Now $\frac{dy'}{dx} = \tan\phi = \phi$ for small values of ϕ then

$$\phi = \frac{2\frac{y'}{x}}{1 - \left(\frac{y'}{x}\right)^2}$$

When $\phi = \phi_e,\ y' = y'_e,\ x = x_e = \frac{c}{2}$ and $z = \frac{a}{c} = \frac{y'_e}{c}$ then

$$\phi_e = \frac{2\frac{y'_e}{c/2}}{1 - \left(\frac{y'_e}{c/2}\right)^2} = \frac{4\frac{y'_e}{c}}{1 - 4\left(\frac{y'_e}{c}\right)^2}$$

$$\phi_e = \frac{4z}{1-4z^2}$$

For denominator values close to the value of 1.0, an alternate equation can be used.

$$\phi_e = 4z\left(1+4z^2\right)$$

Using the new equation for ϕ_e for circular arc camber, the corresponding lift and pitching-moment coefficient equations are:

$$C_l = 4\pi z\left(1+4z^2\right)$$
$$C_{m_{c/4}} = -\pi z\left(1+4z^2\right)$$

The factor $\left(1+4z^2\right)$ indicates that for 2% camber, the increase in the aerodynamic coefficients is of the order of one-sixth of one percent of the original value $\left[\left(1+4z^2\right)=1.0016\right]$. This small amount is also the difference in the aerodynamic results between airfoils using circular arc and parabolic arc camber.

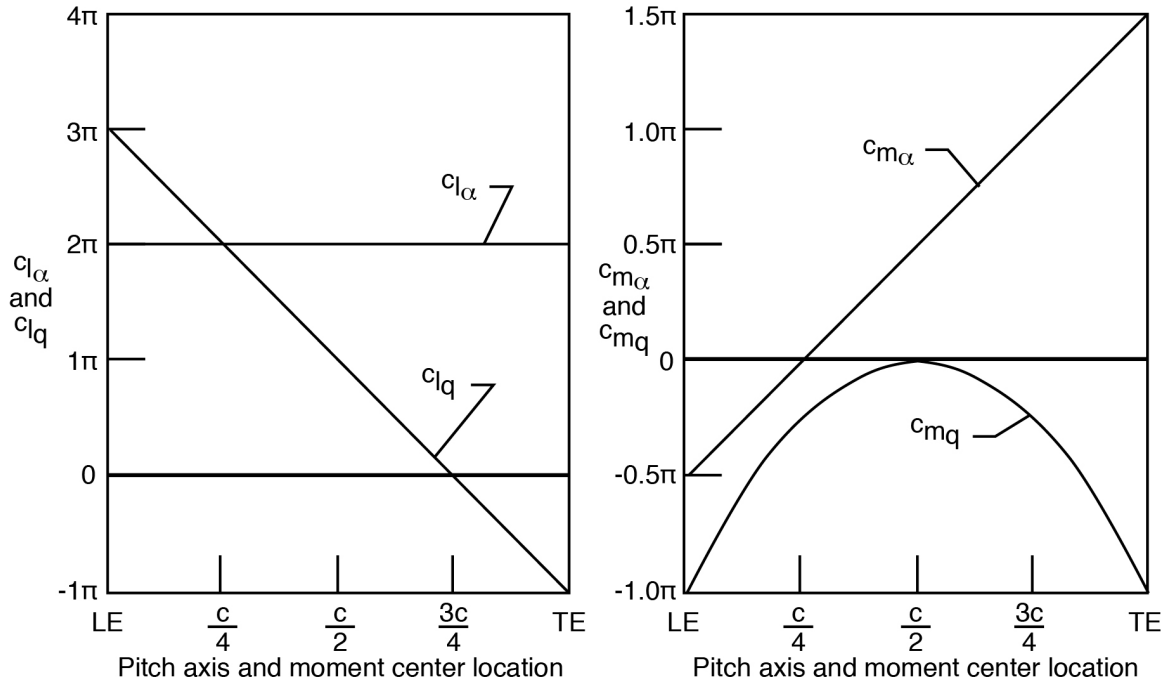

Figure 1. Thin airfoil theory results

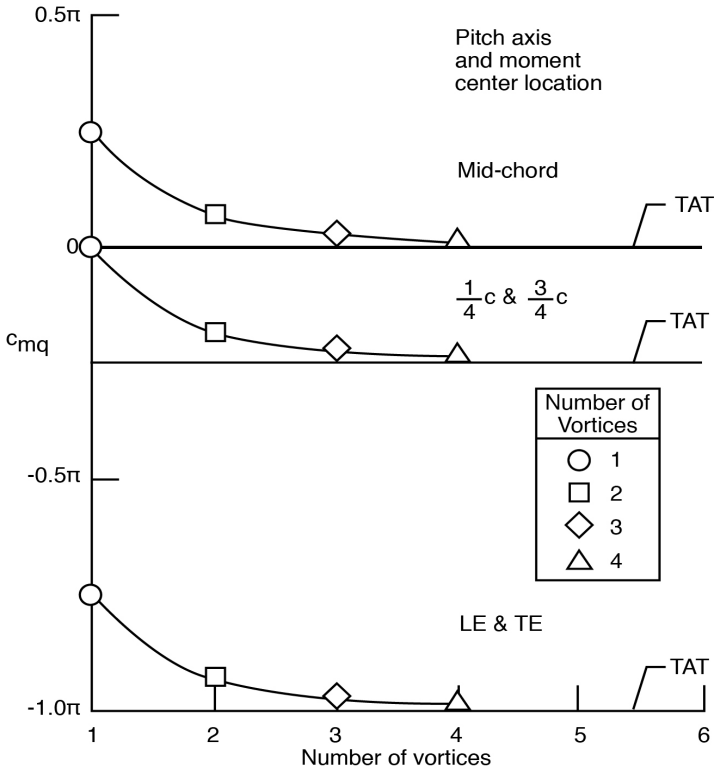

Figure 2. Effect on pitch damping of the number of vortices representing the airfoil

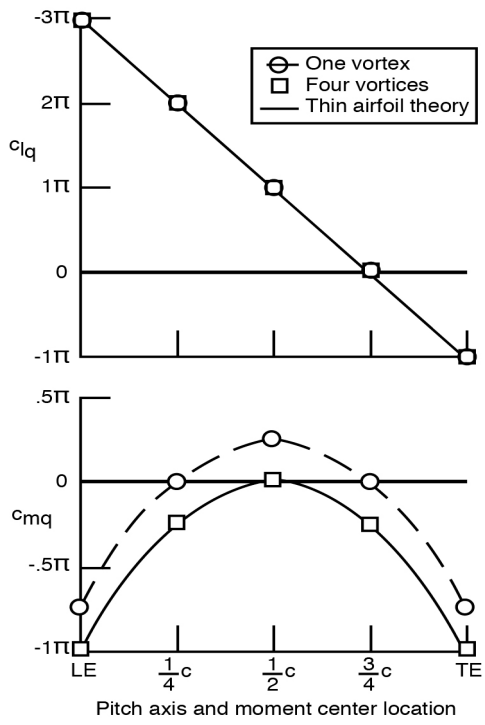

Figure 3. Comparison of discreet vortex calculated values with thin airfoil theory results

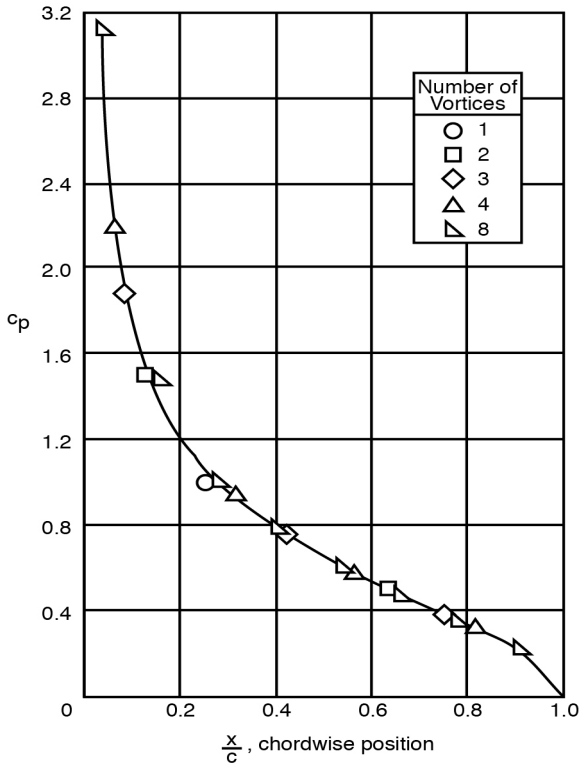

Figure 4. Chordwise pressure distribution for $\alpha = 1/2\pi$

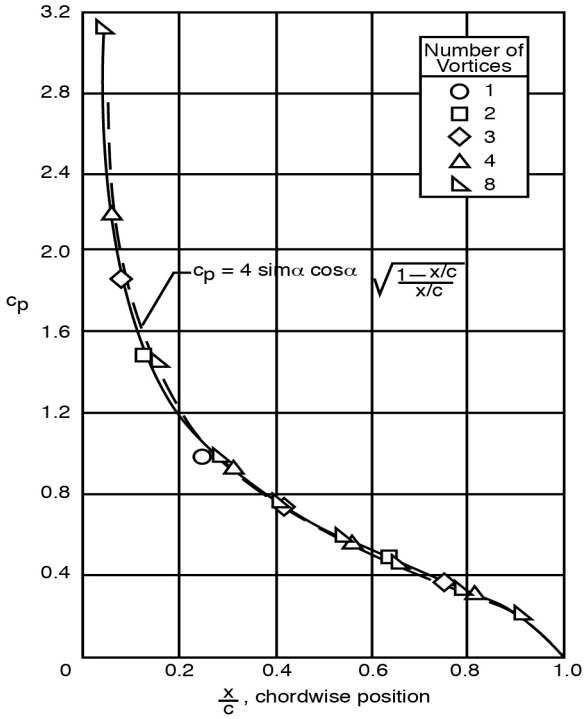

Figure 5. Comparison of chordwise pressure distributions for two methods ($\alpha = 1/2\pi$ rad)

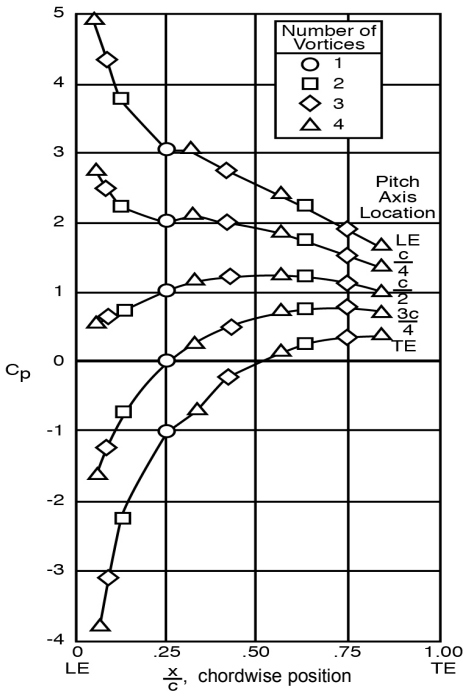

Figure 6. Chordwise pressure distribution for $qc/2V = 1/\pi$

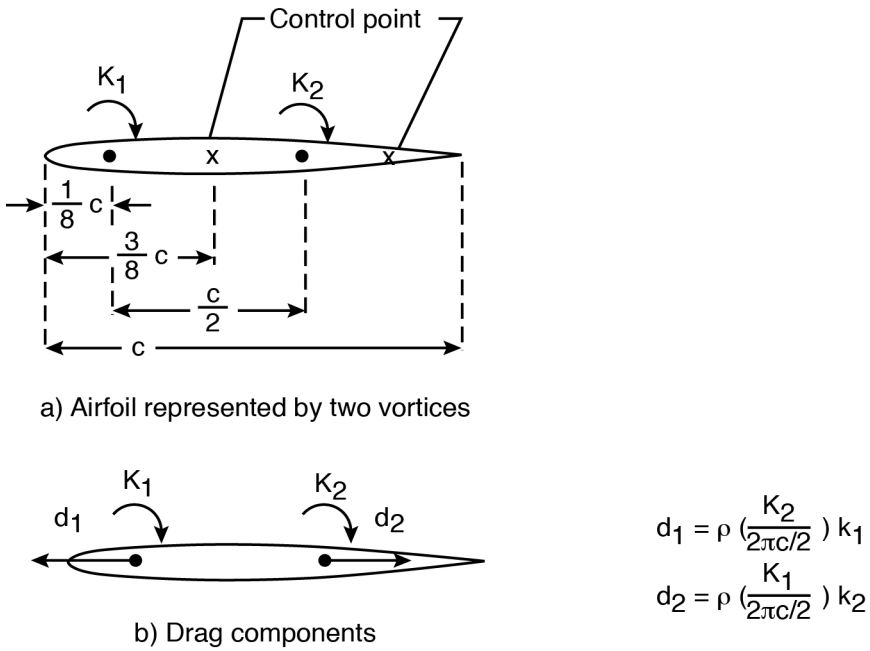

Figure 7. Sketches used in airfoil drag computation

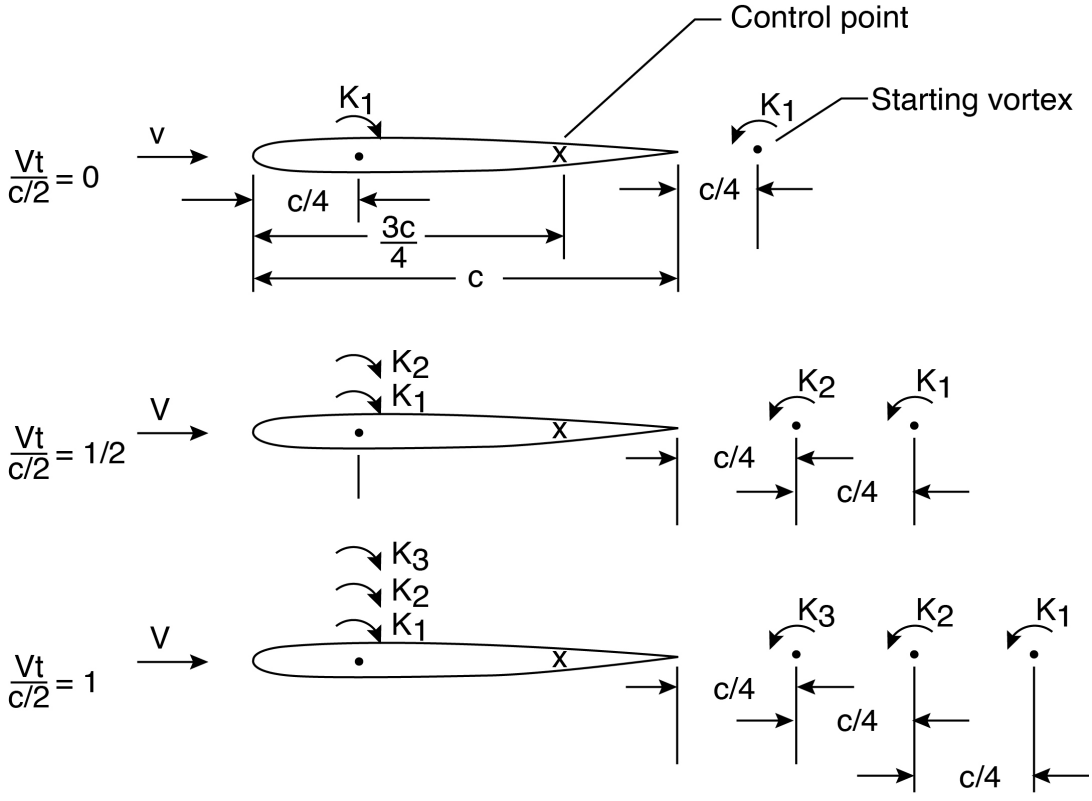

Figure 8. Sketches illustrating locations of the incremental vortices for airfoil and wake with increasing time (Single resultant vortex represents the airfoil)

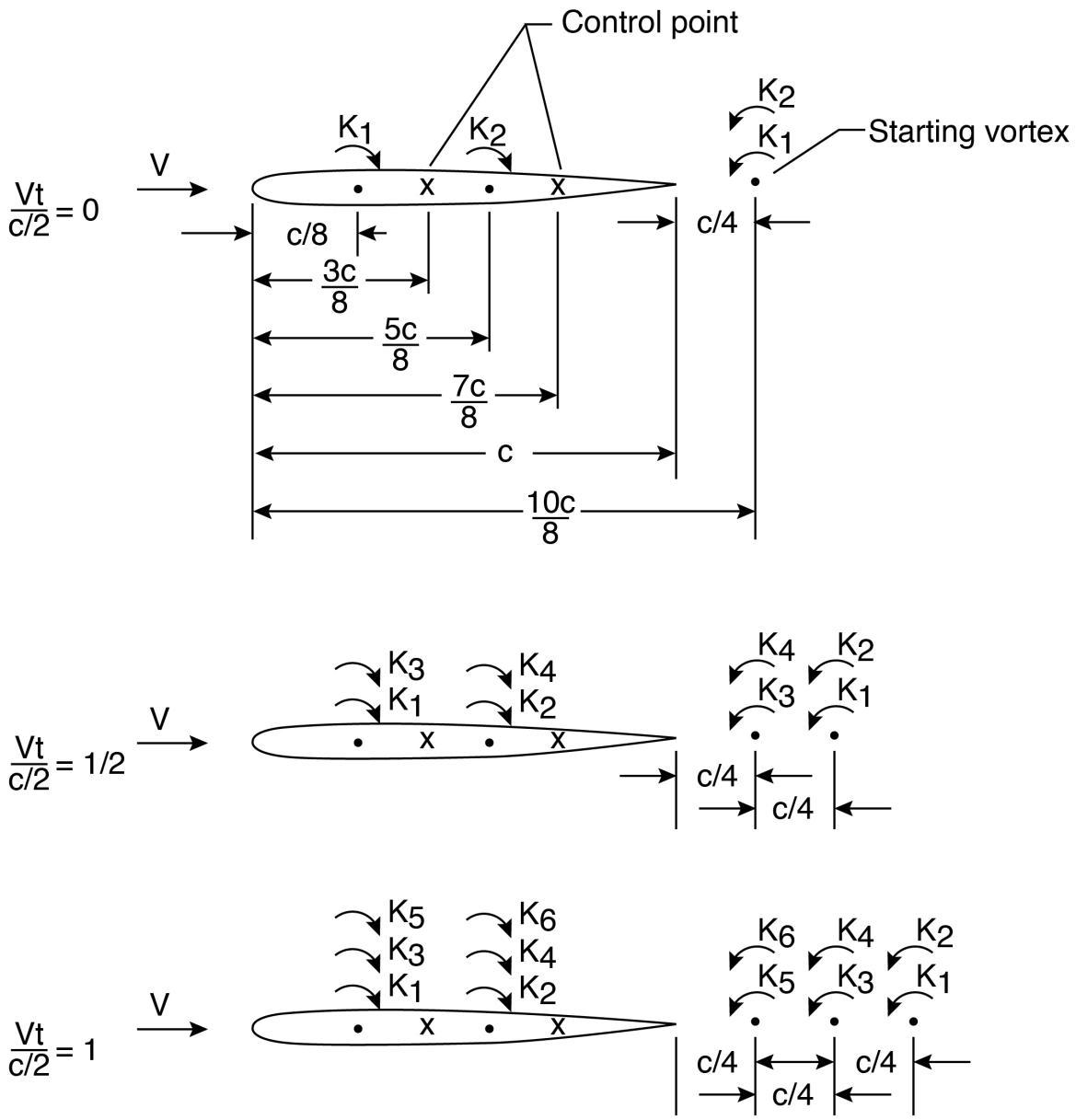

Figure 9. Sketches illustrating an improved arrangement (Two resultant vortices represent the airfoil)

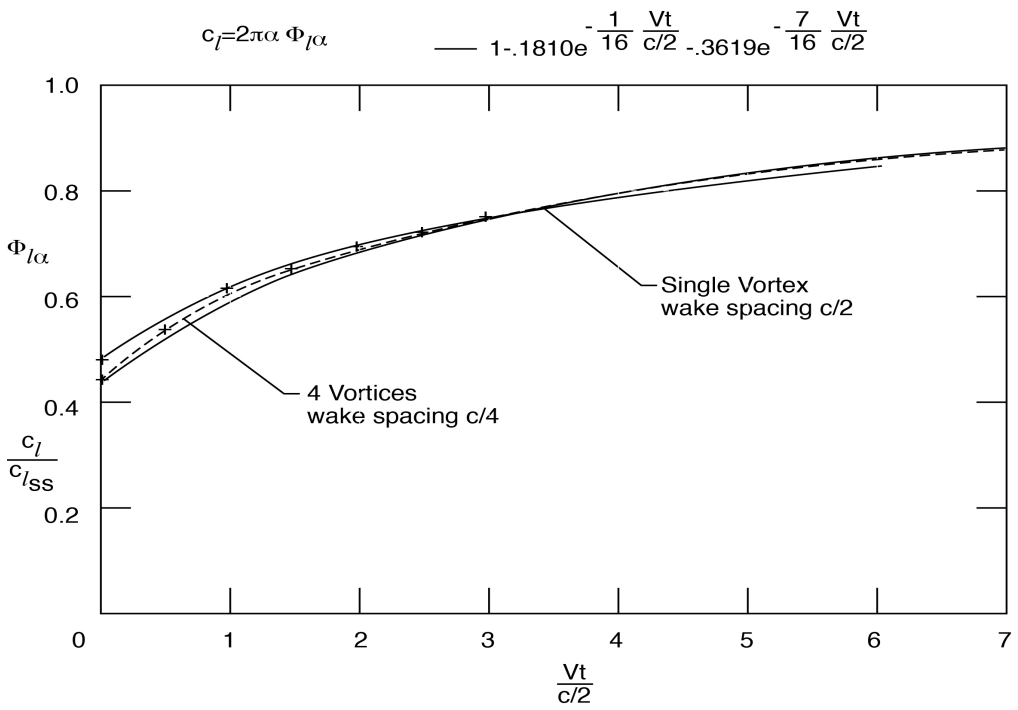

Figure 10. Lift indicial response due to angle of attack

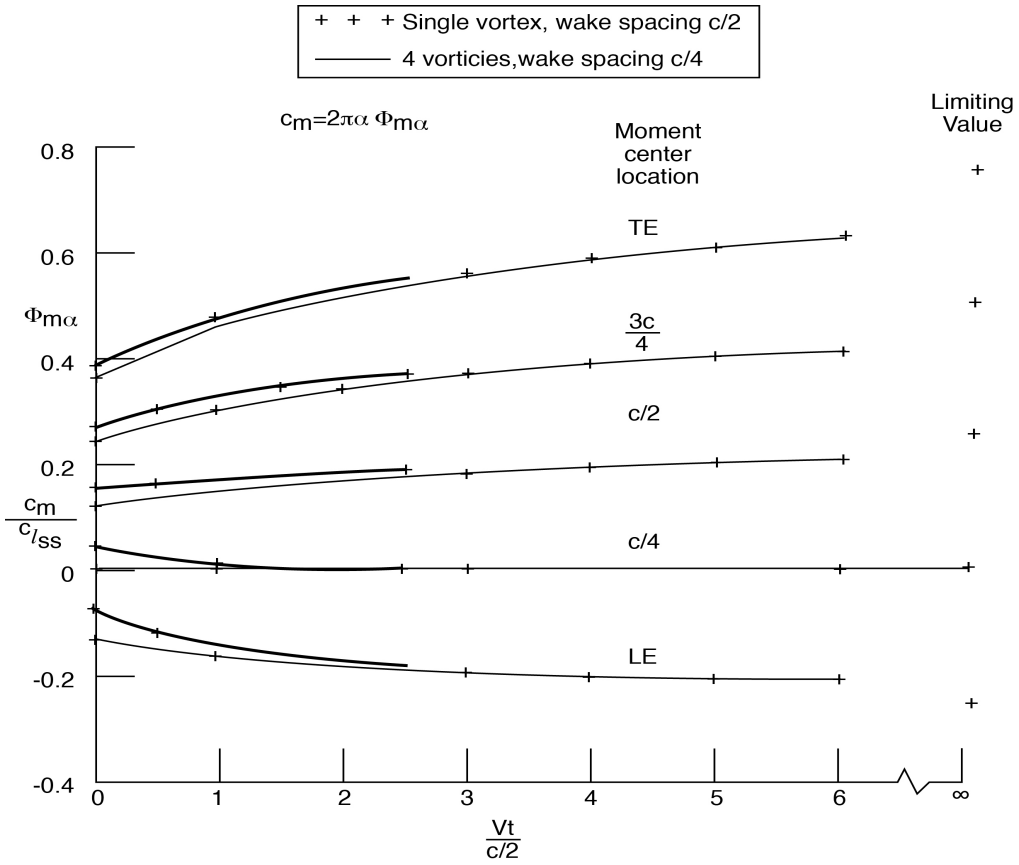

Figure 11. Pitching moment indicial response due to angle of attack

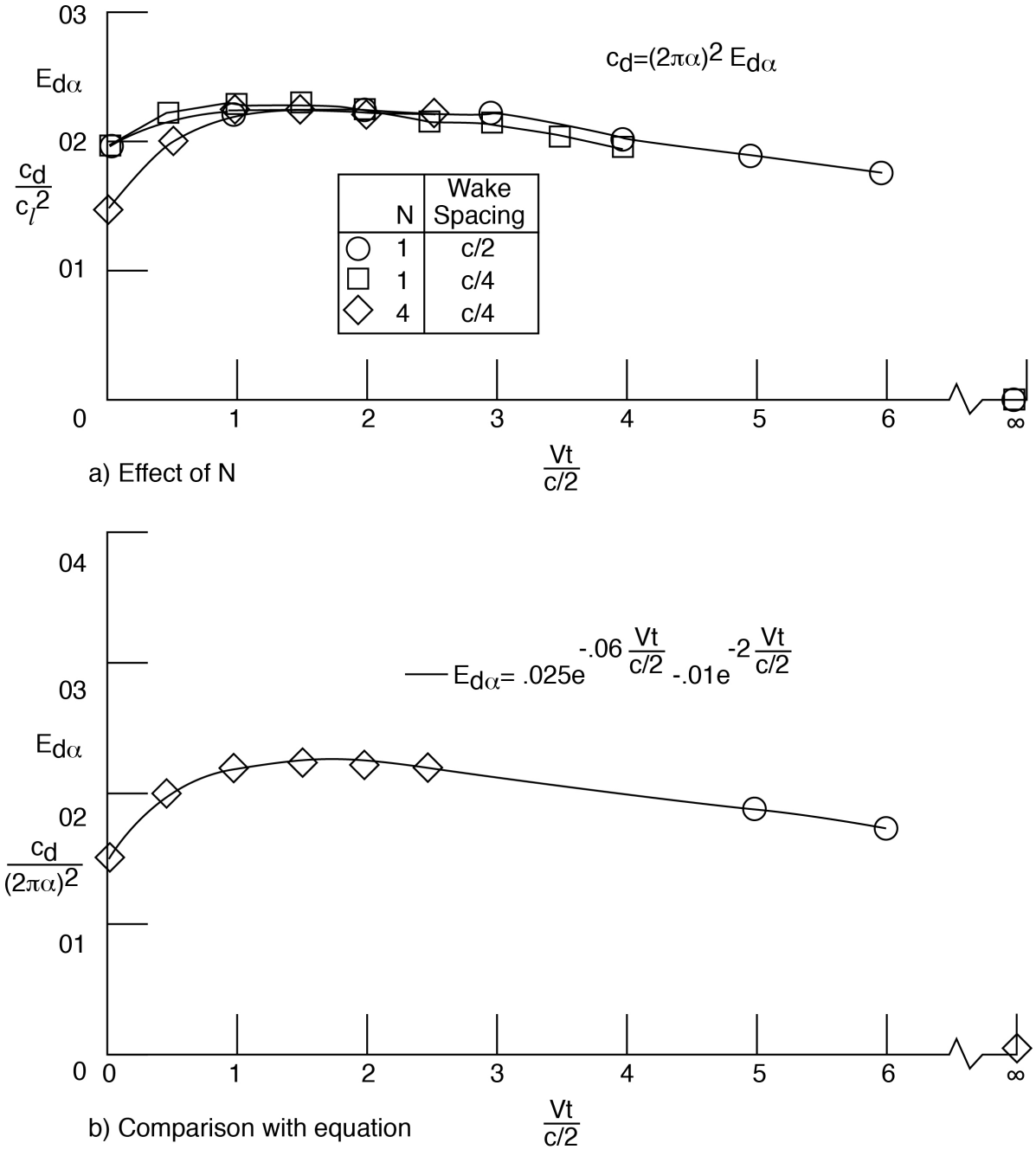

Figure 12. Response of induced drag function due to a step input in α

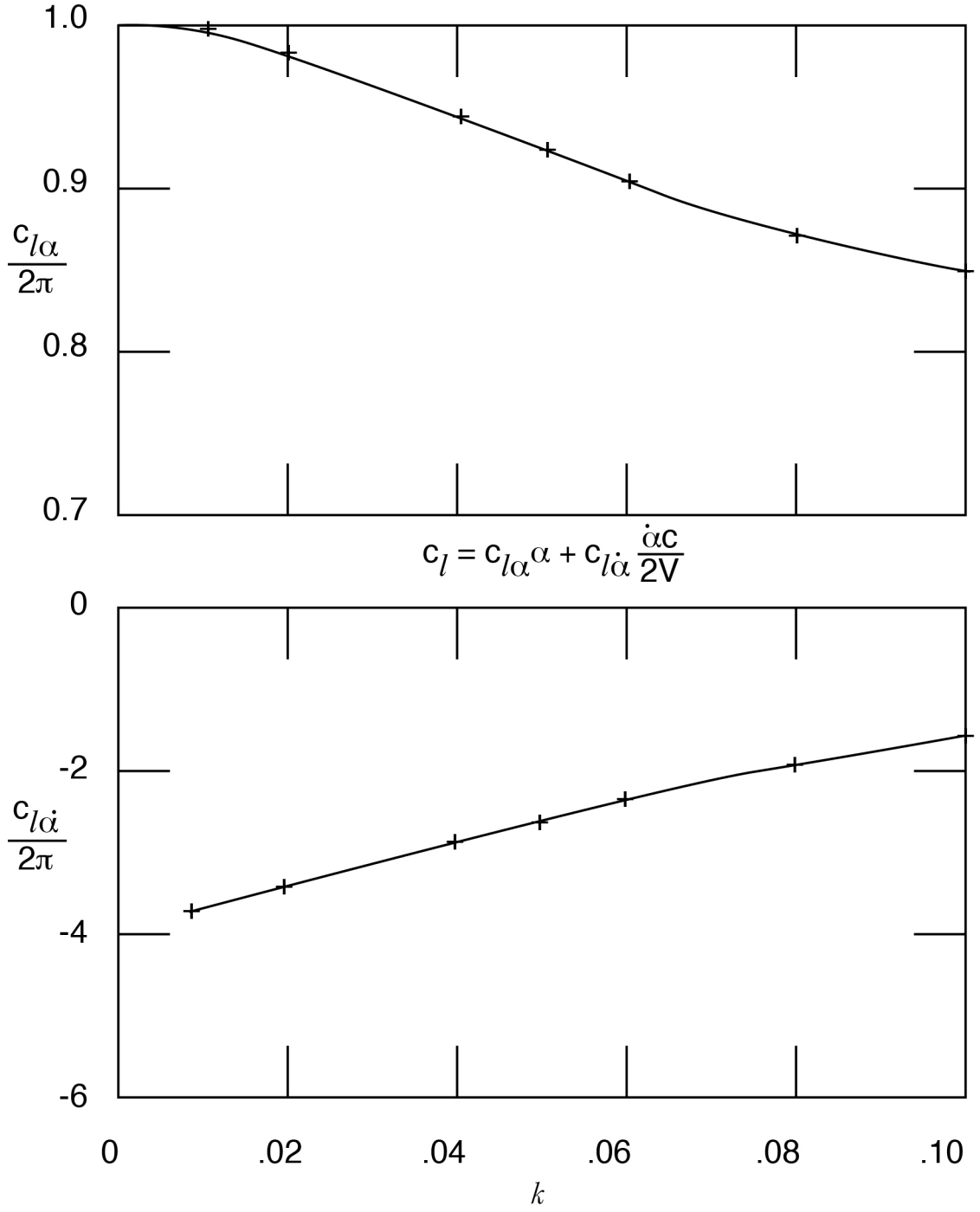

Figure 13. Lift derivatives for sinusoidal oscillations in angle of attack

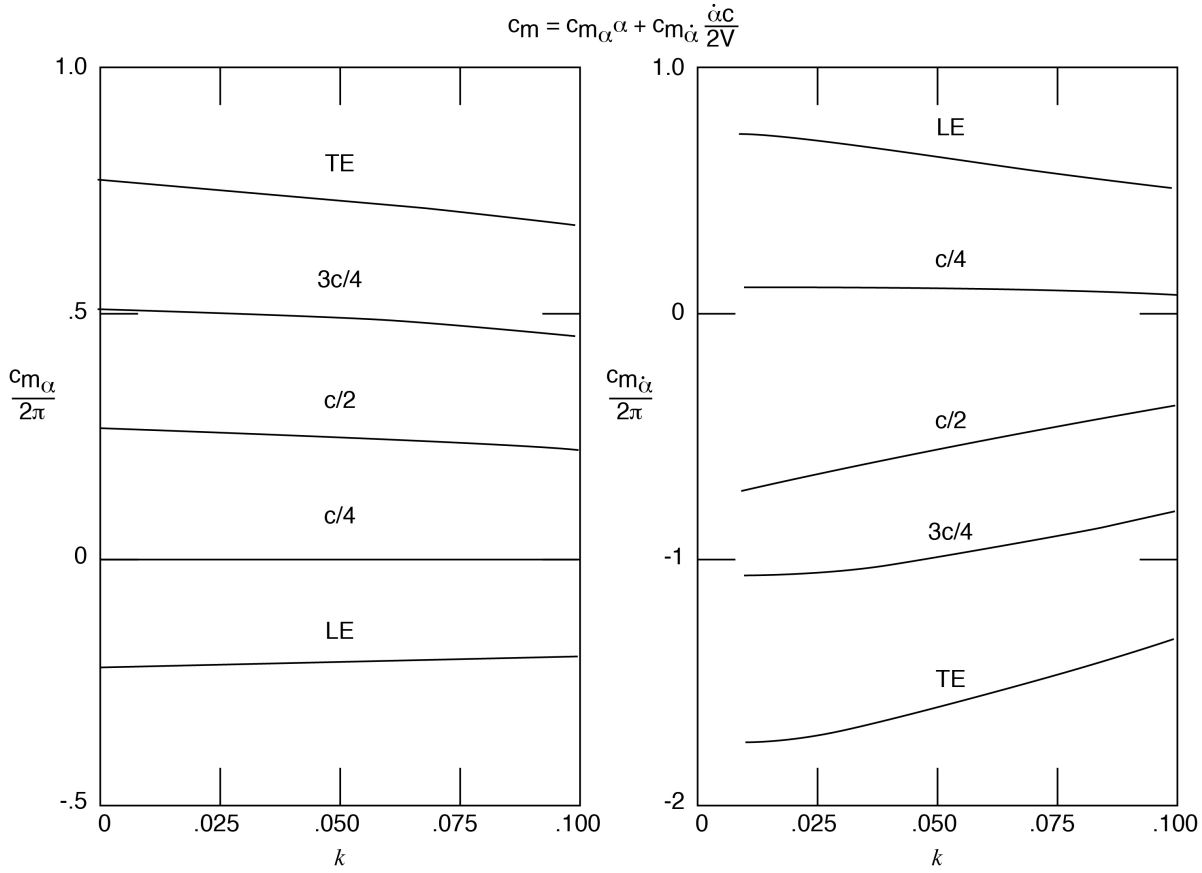

Figure 14. Moment derivatives for sinusoidal oscillations in angle of attack for 5 chordwise locations of the moment center.

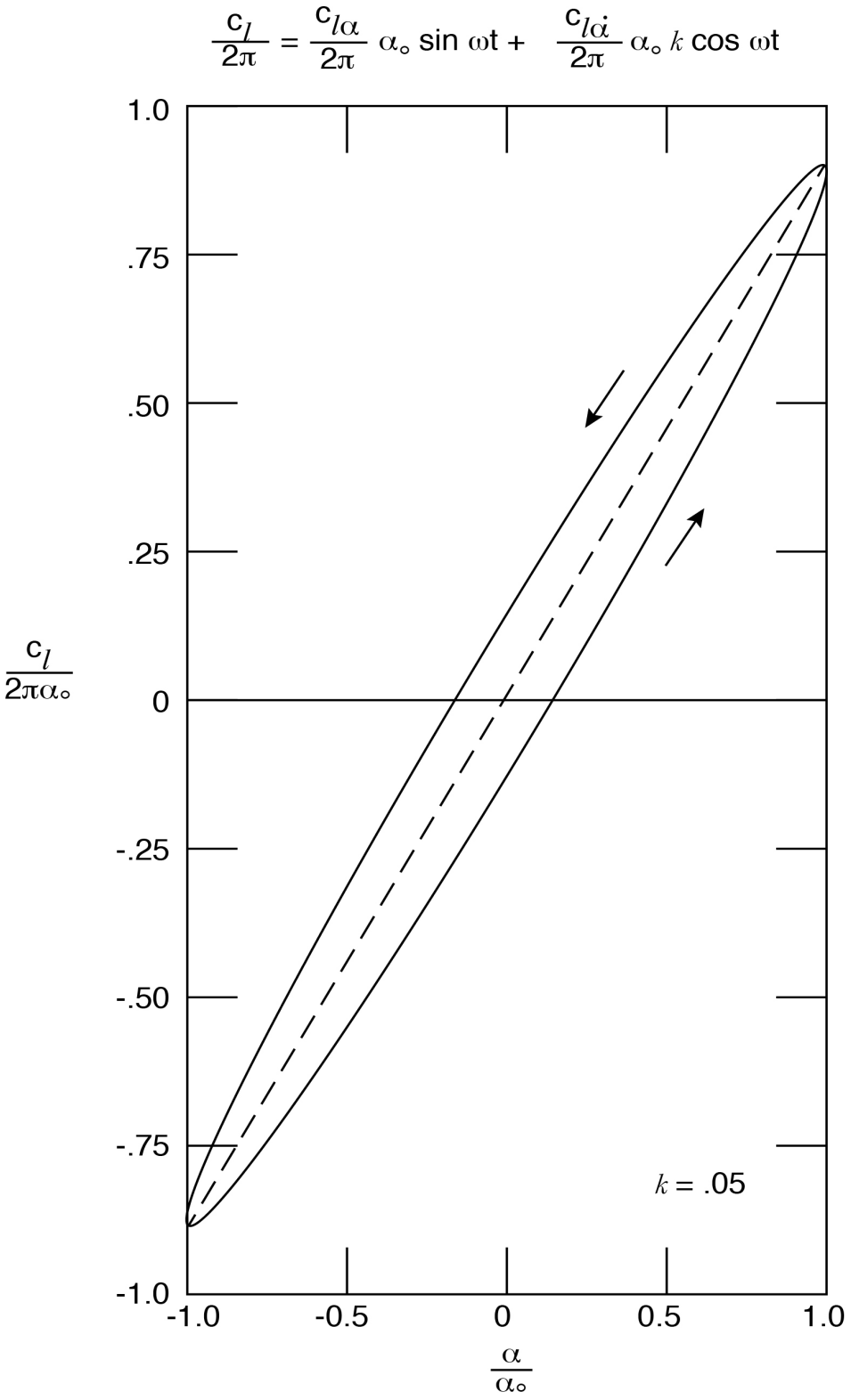

Figure 15. Lift – displacement trace for sinusoidal plunging oscillation

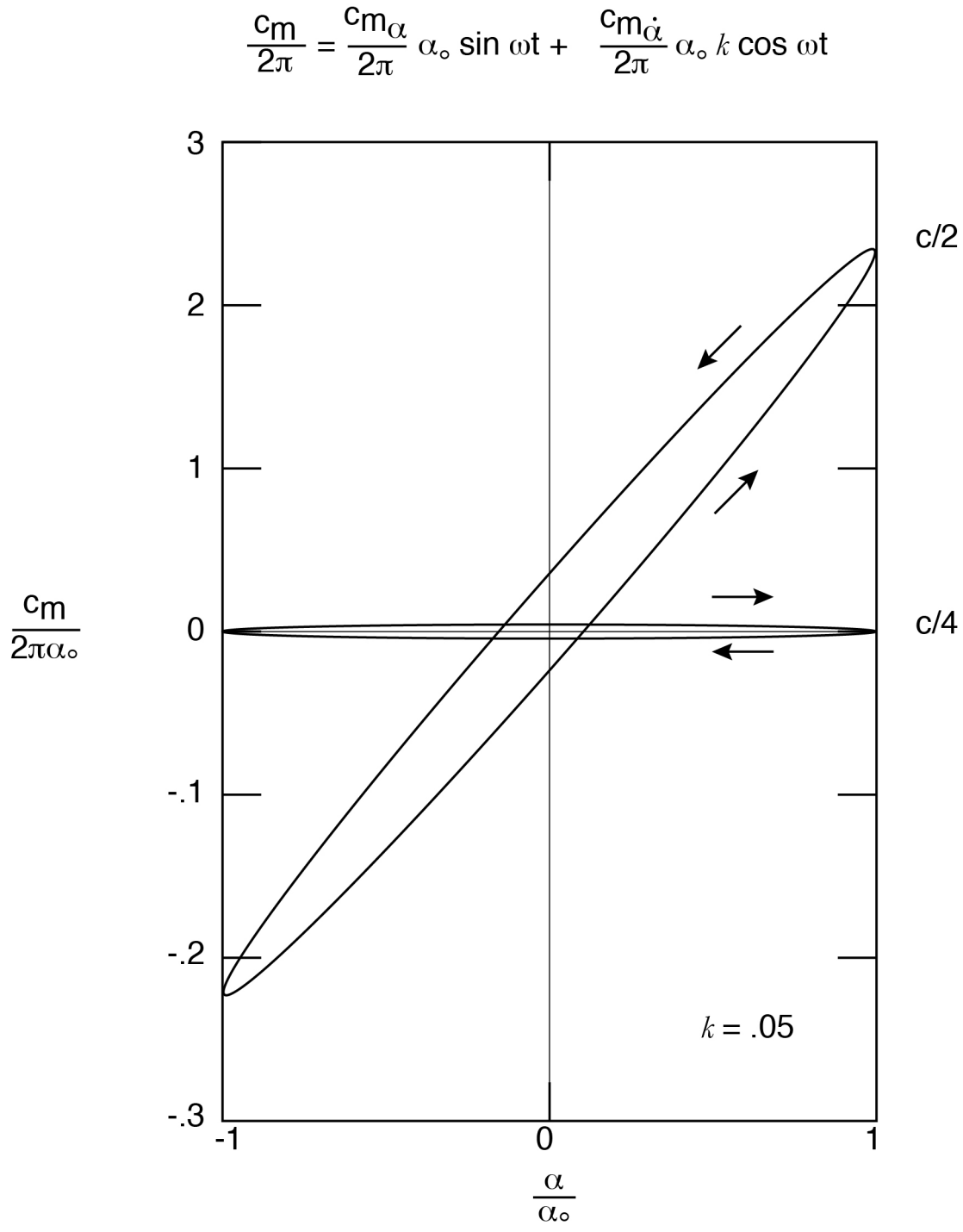

Figure 16. Moment – displacement trace for a sinusoidal plunging oscillation

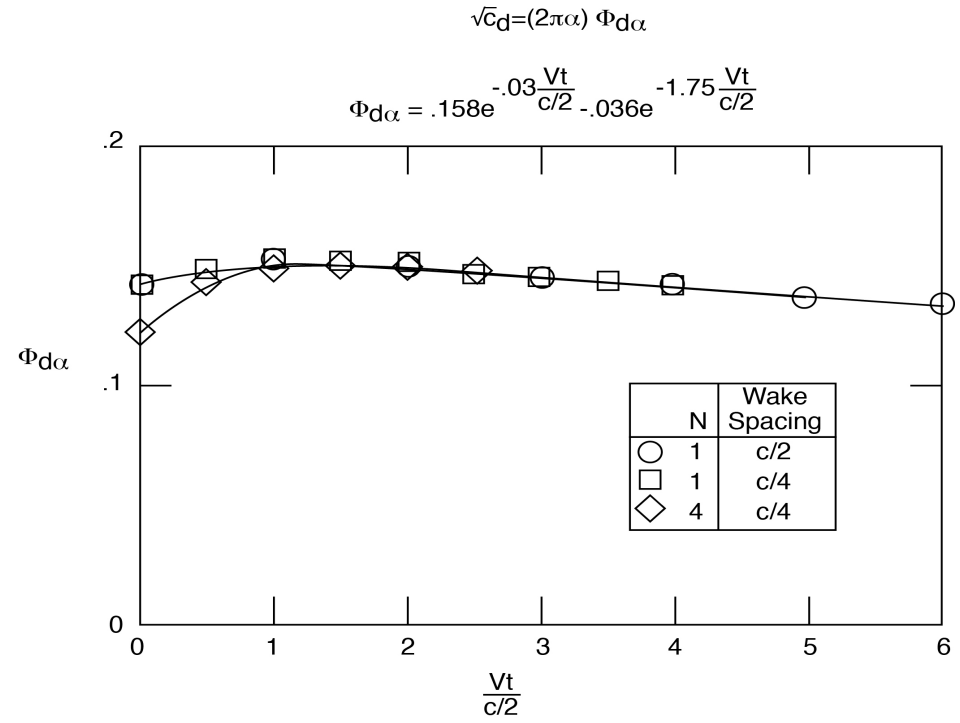

a. Indicial function curve

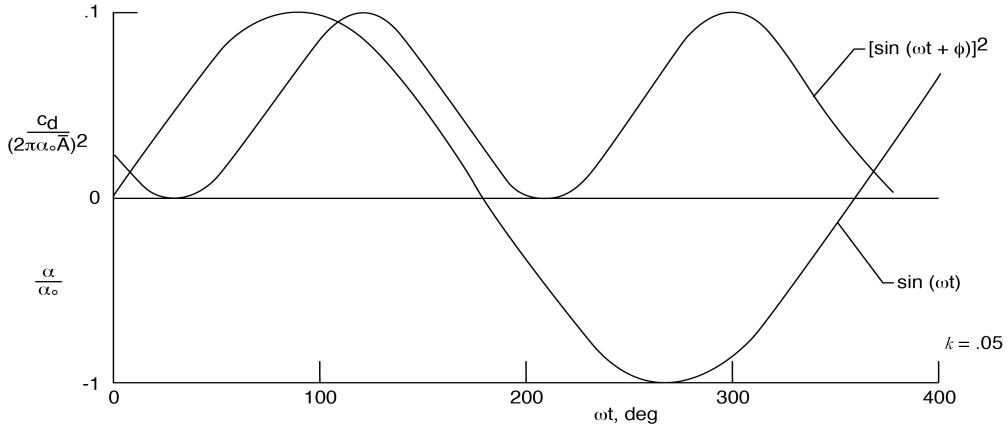

b. Time history responses

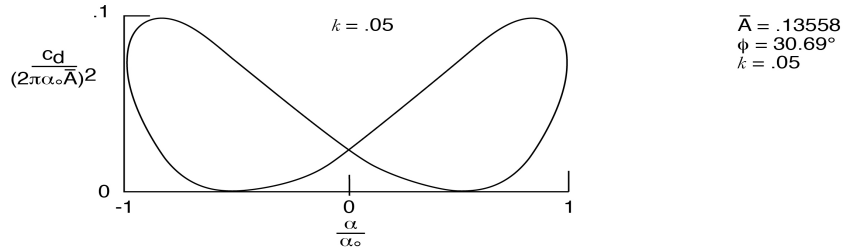

c. Induced drag displacement trace for sinusoidal plunging oscillation

Figure 17. Development curves for induced drag information

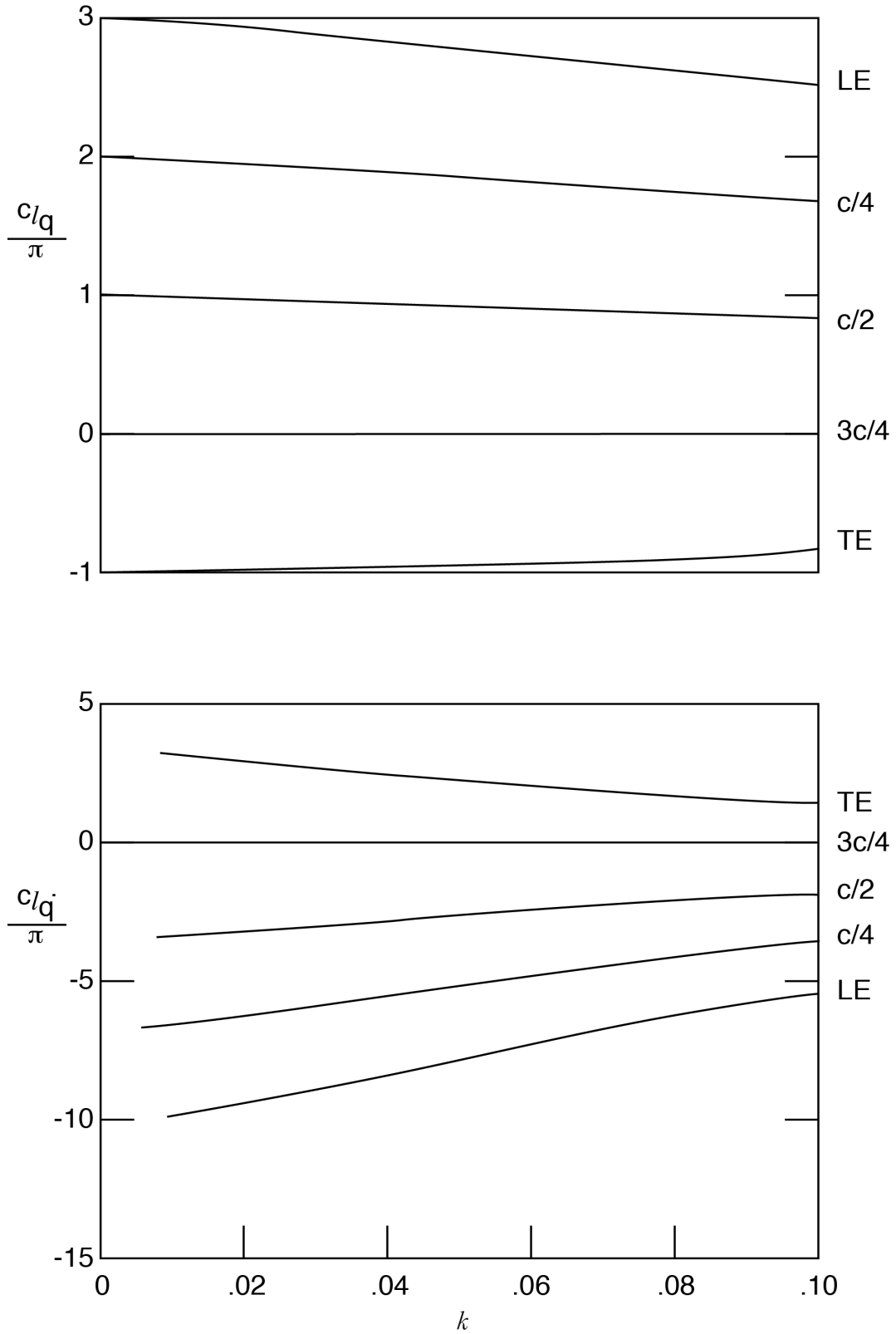

Figure 18. Lift derivatives for sinusoidal oscillations in pitch rate holding angle of attack constant at zero

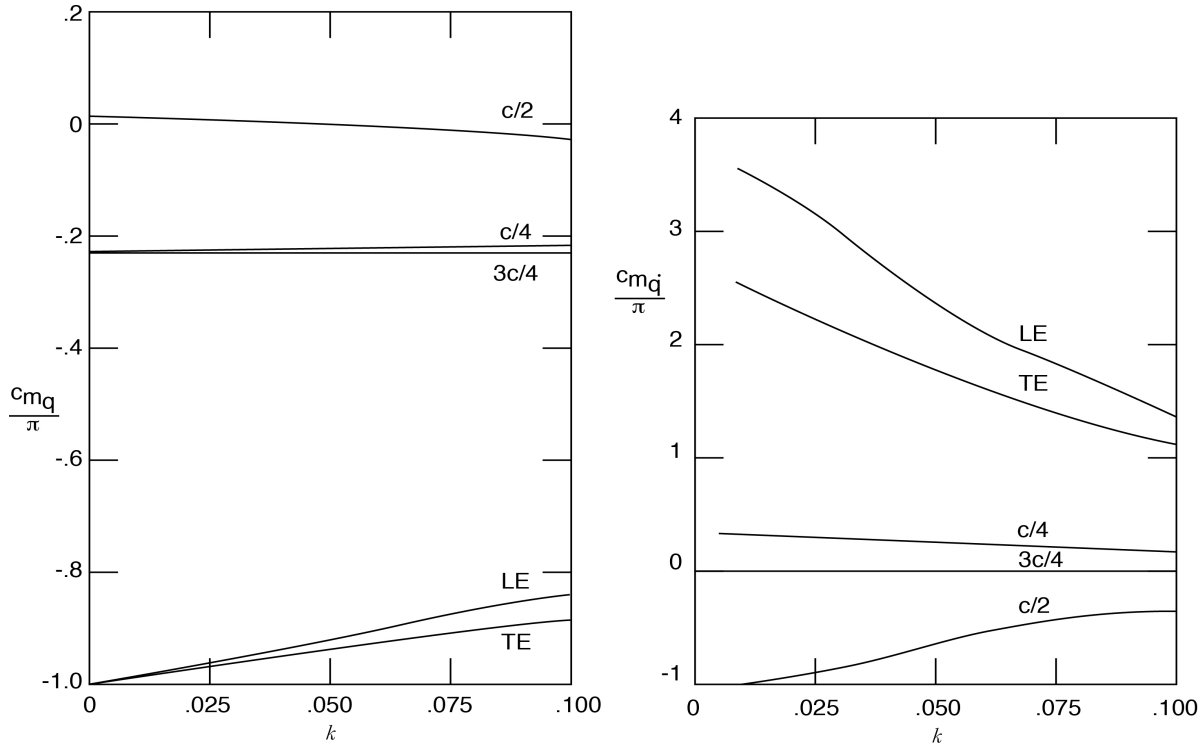

Figure 19. Pitching moment derivatives for sinusoidal oscillations in pitch rate holding angle of attack constant at zero

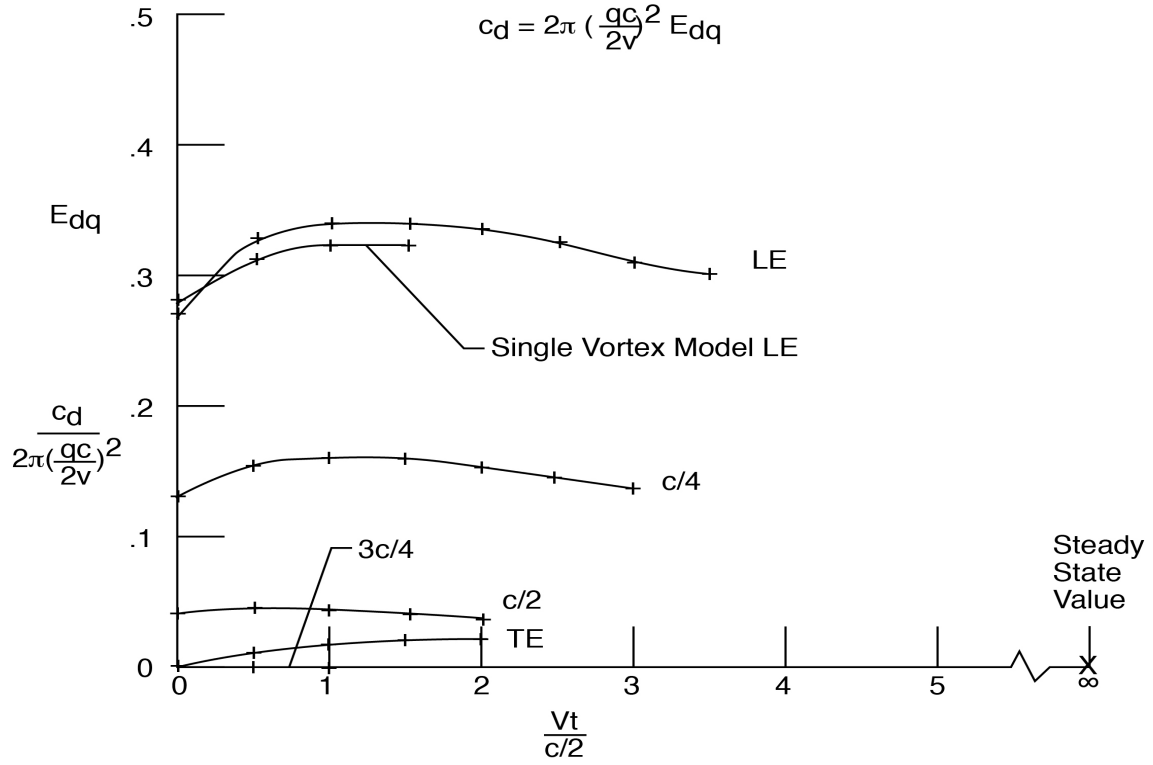

Figure 20. Induced drag function step input response to pitch rate for various pitch axis locations with N=4 (angle of attack held constant at zero)

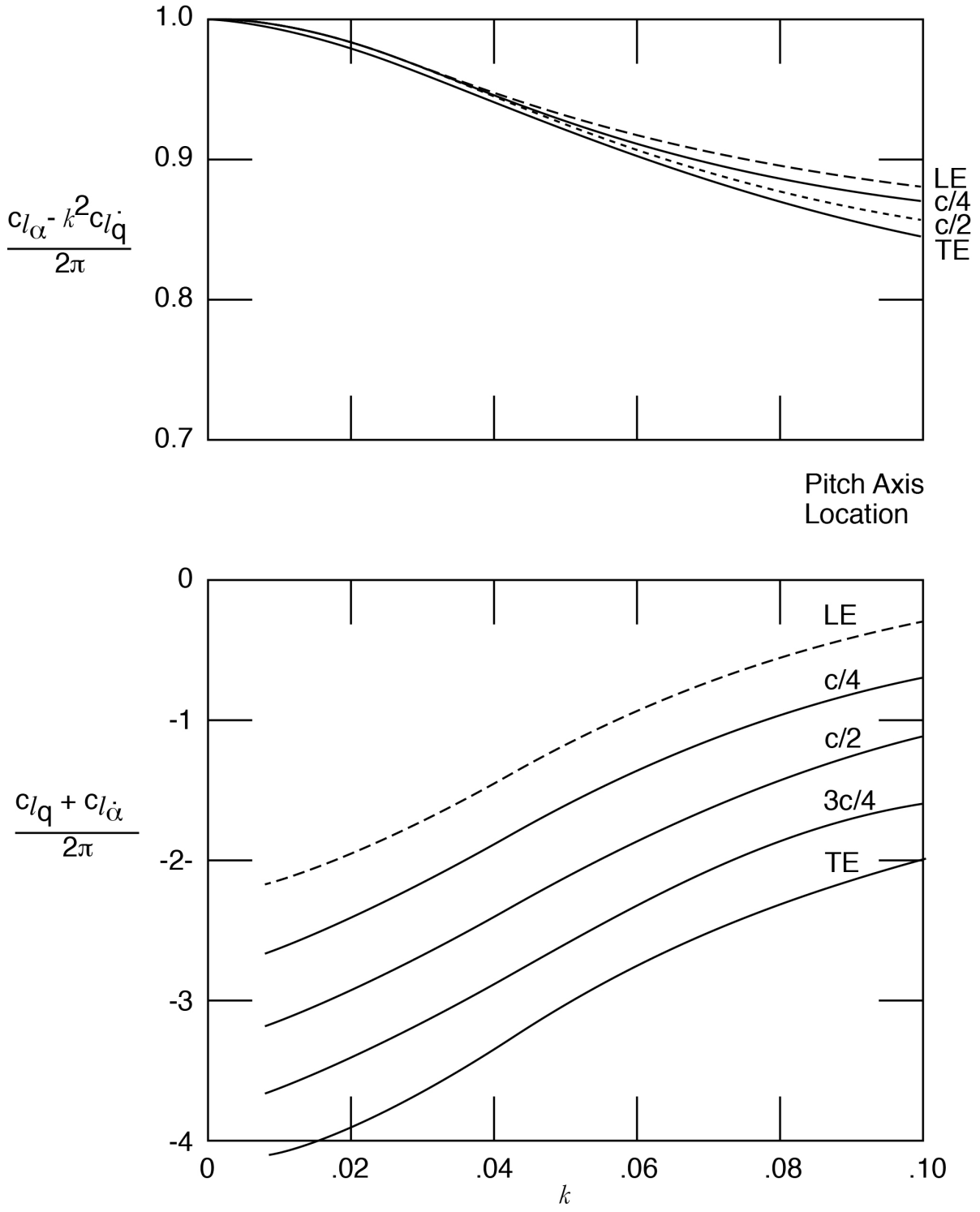

Figure 21. Calculated aerodynamic derivatives for lift of a thin two-dimensional airfoil oscillating sinusoidally in pitch about an axis on the chord

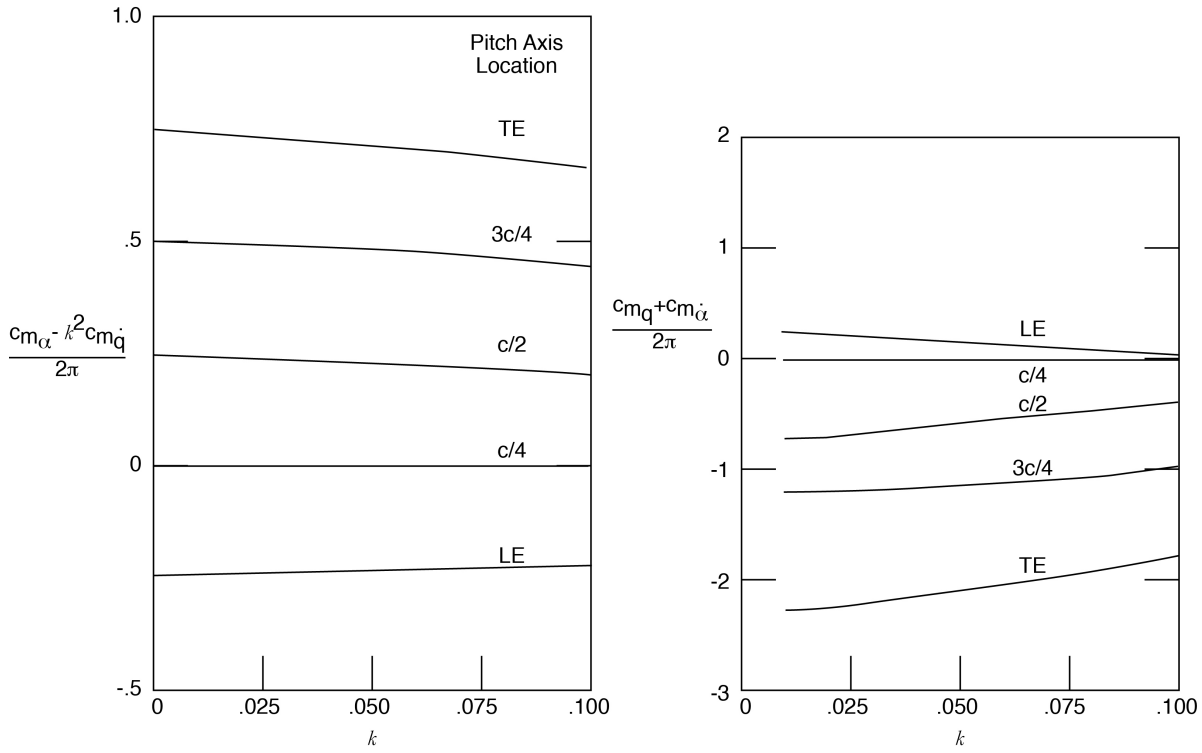

Figure 22. Calculated aerodynamic derivatives for pitching moment of a thin airfoil oscillating sinusoidally in pitch about an axis on the chord

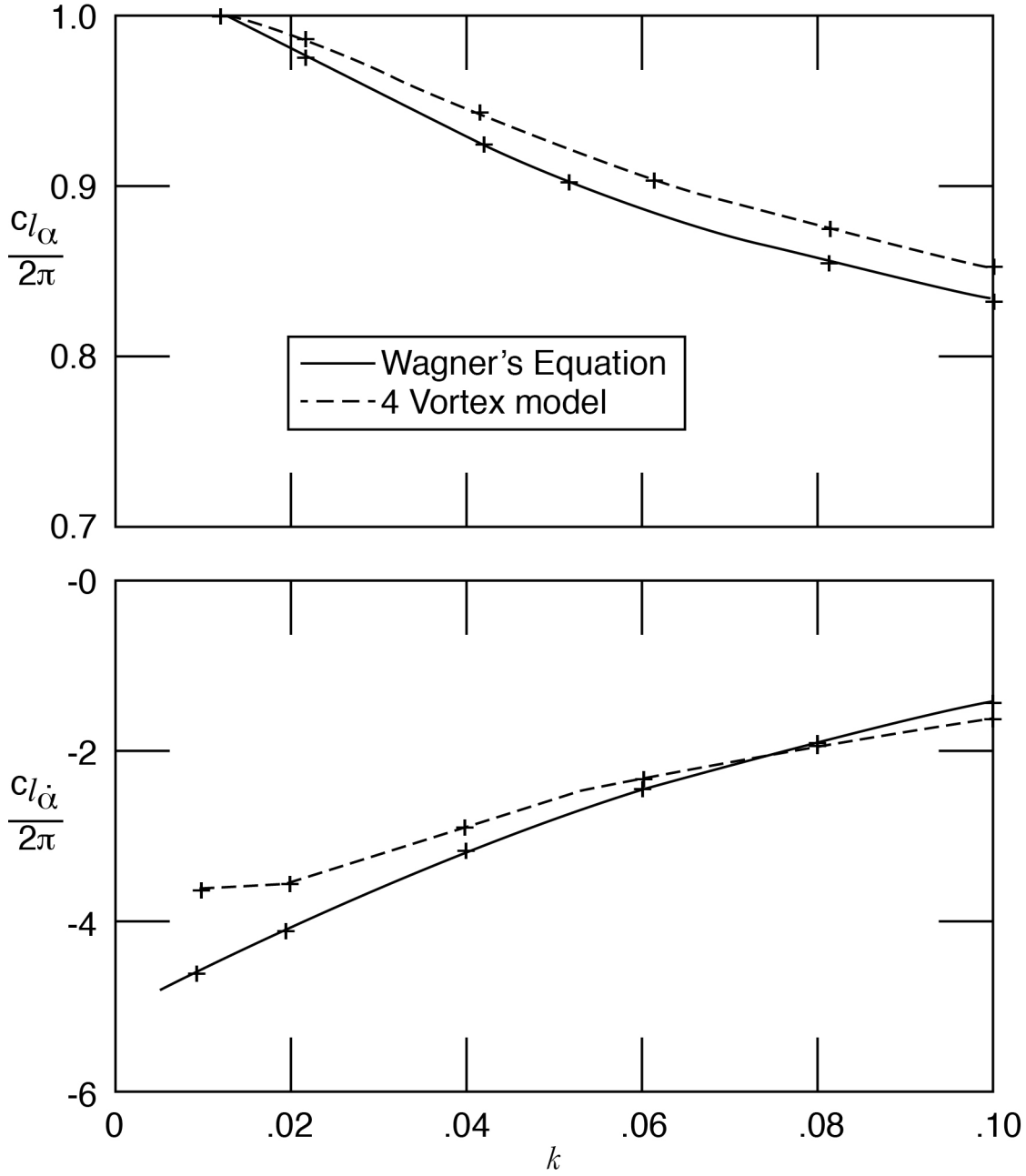

Figure 23. Comparison of results using Wagner's equation with 4-vortex model results

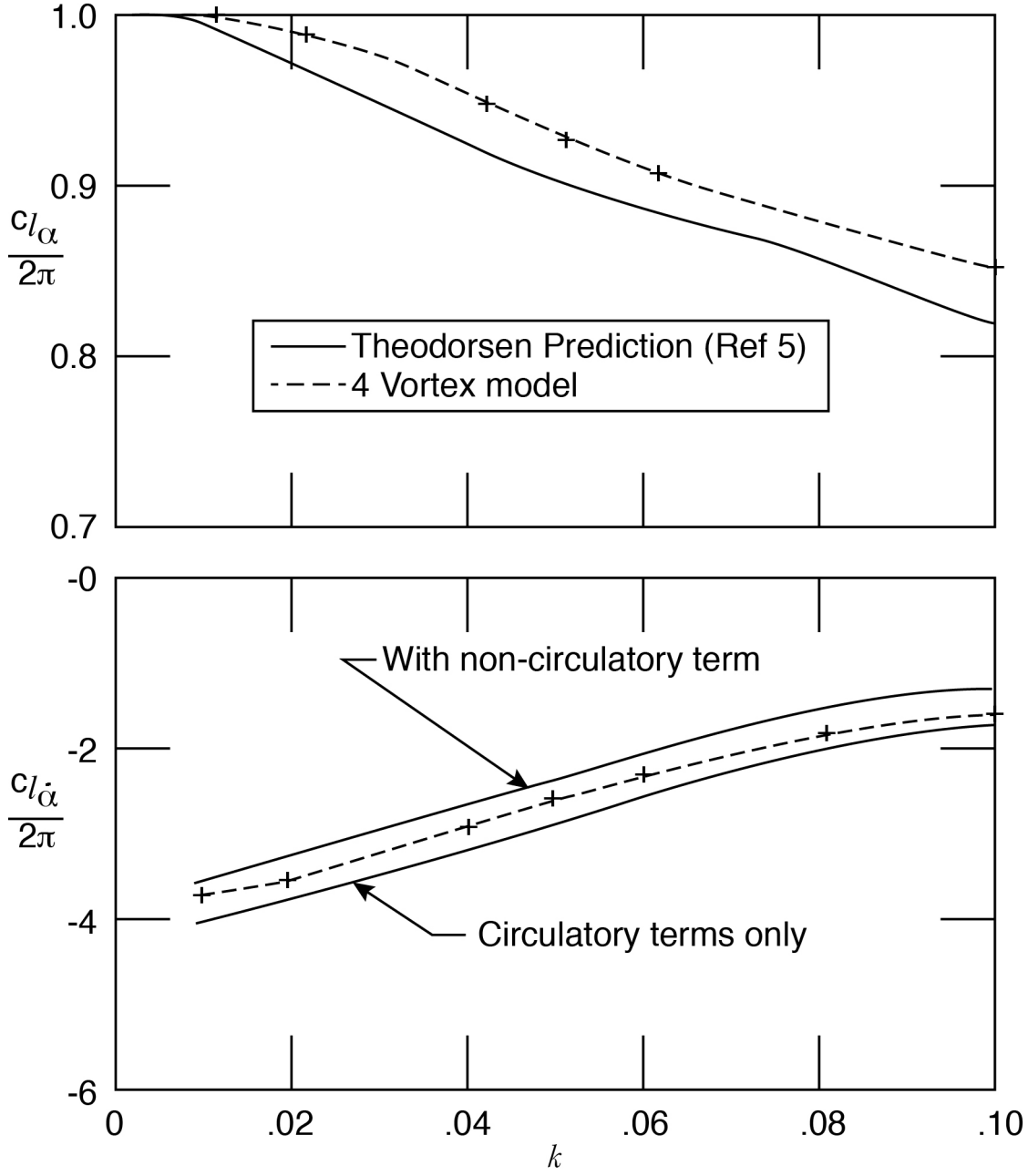

Figure 24. Comparison of Theodorsen prediction with 4-vortex model results

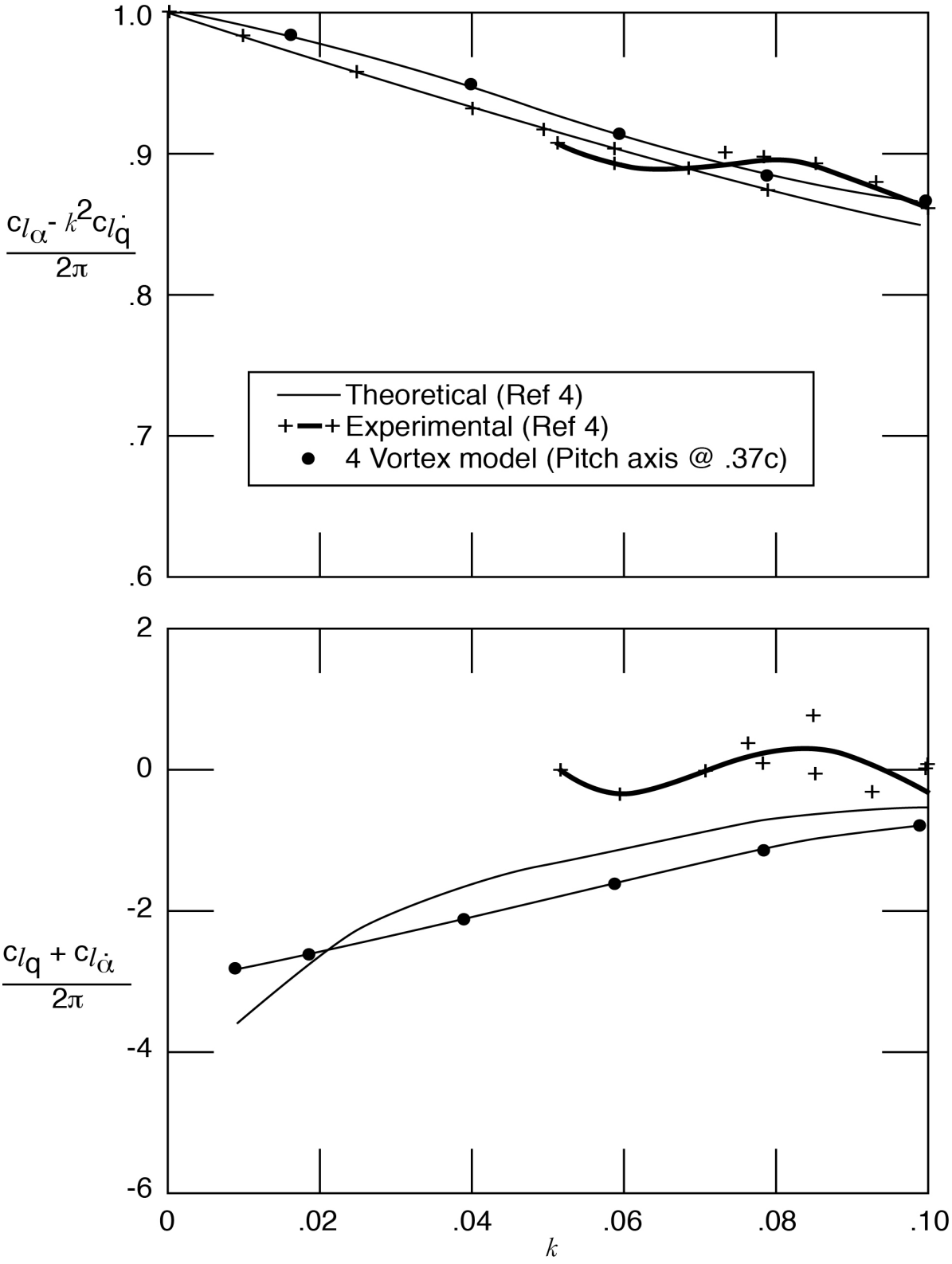

Figure 25. Comparison of TR 1108 results (pitch axis 0.37$\bar{c}$) with experimental results corrected by lift curve slope ratio

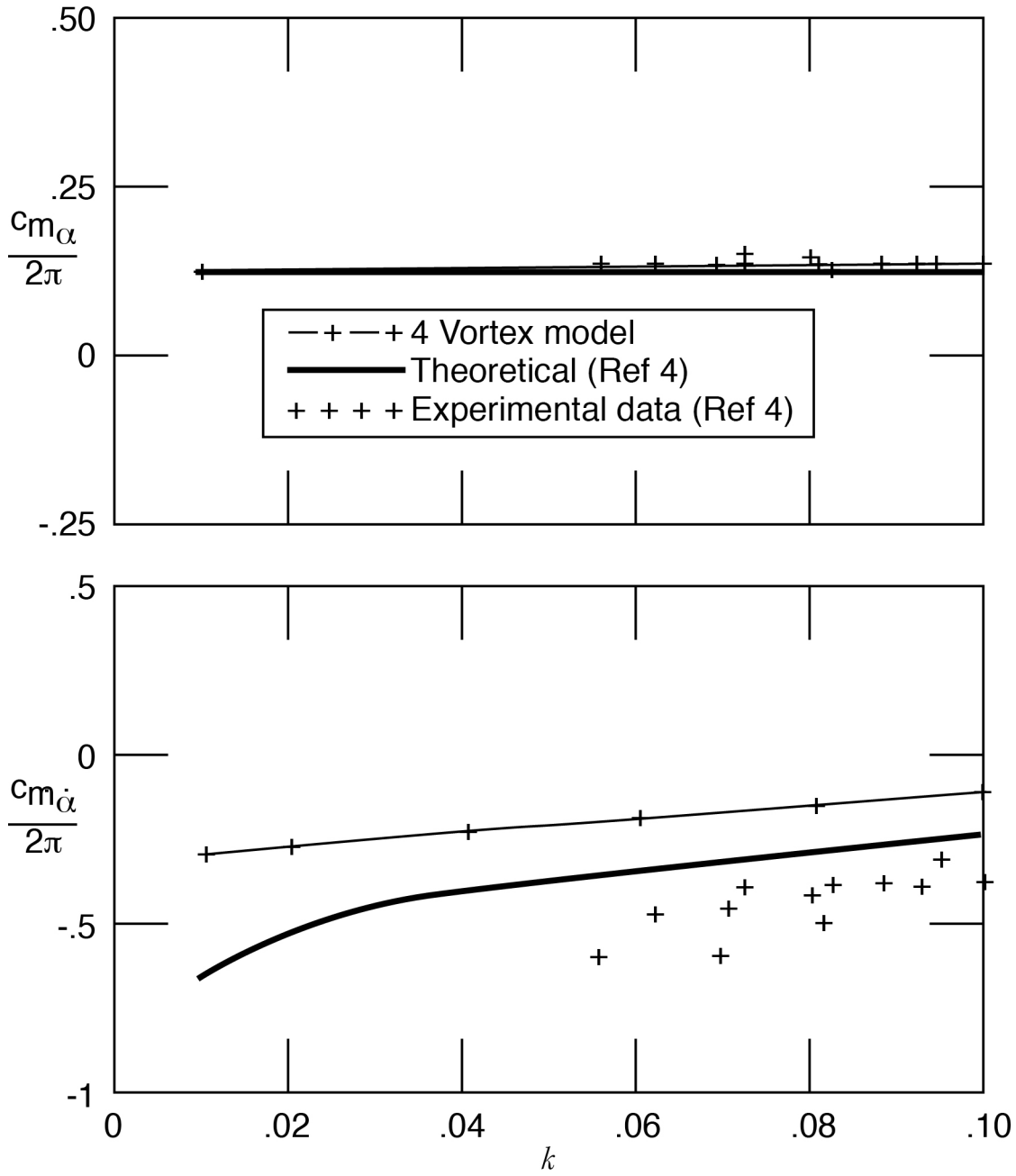

Figure 26. Comparison of TR 1108 results (pitch axis $0.37\bar{c}$) with 4-vortex model predictions

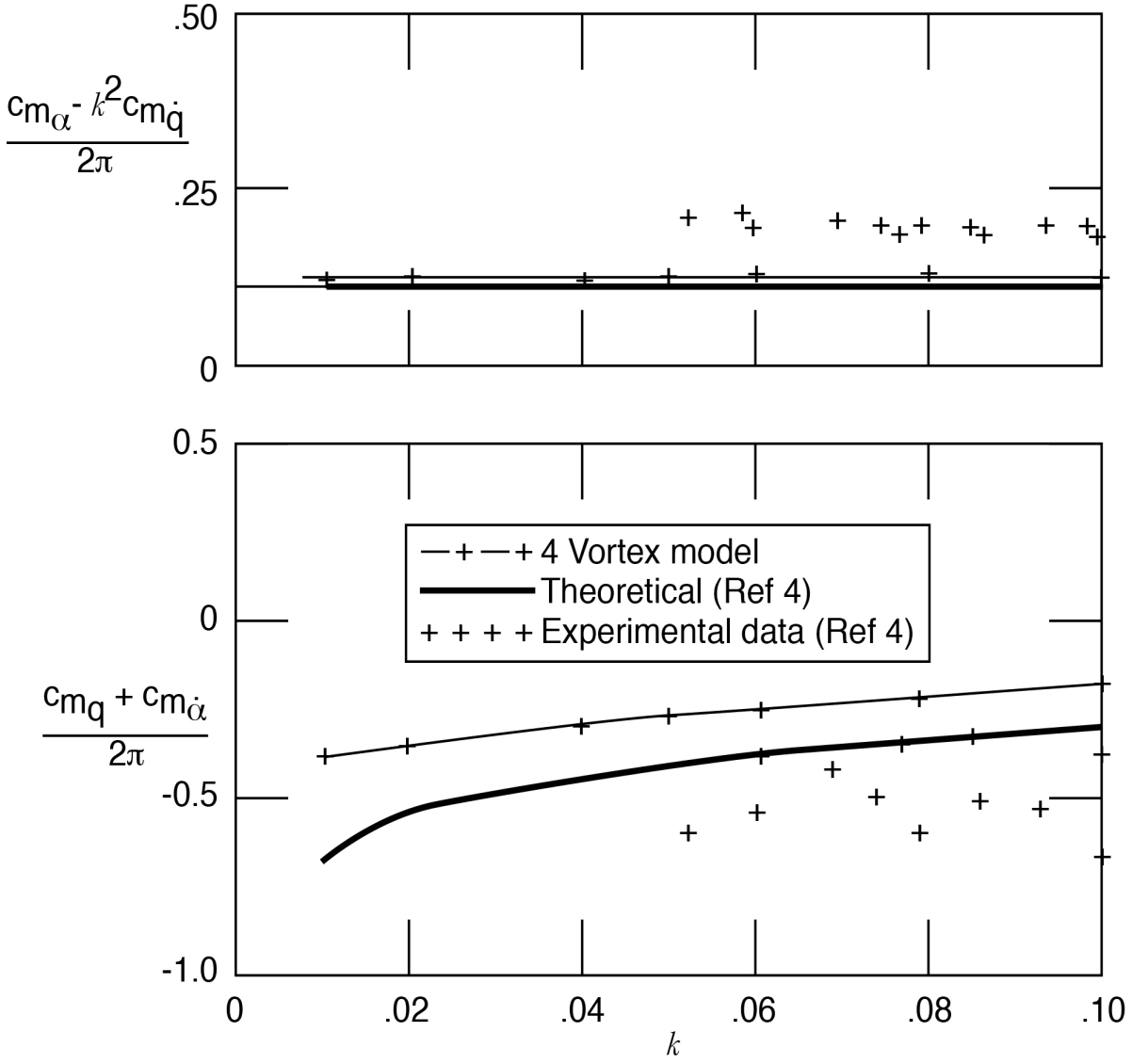

Figure 27. Comparison of TR 1108 combination results (pitch axis 0.37$\bar{c}$) with 4-vortex model predictions

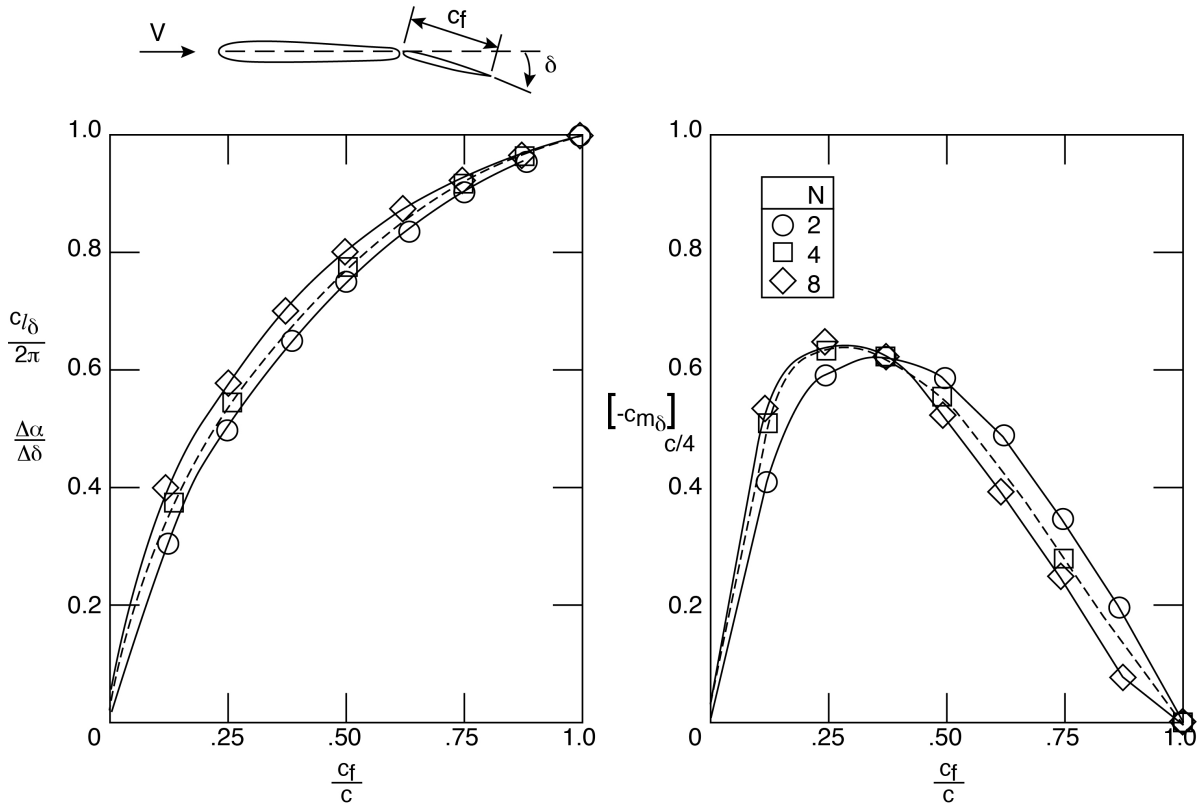

Figure 28. Airfoil steady state lift and moment derivatives due to flap deflection for various values of the ratio of flap chord to airfoil chord (plain flaps with gap sealed)

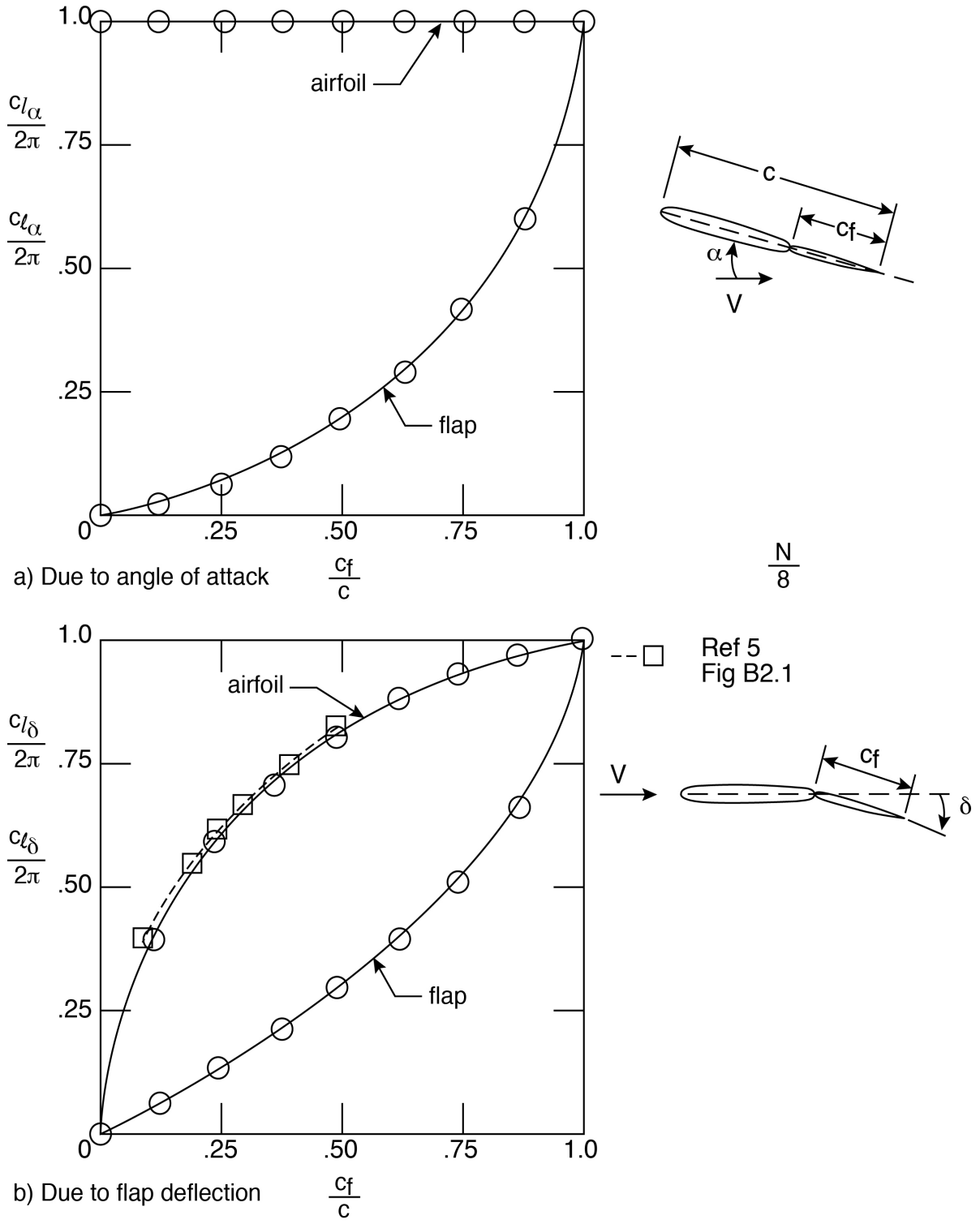

Figure 29. Flap lift to airfoil lift comparison for steady state conditions ($\frac{vt}{c/2} = \infty$)

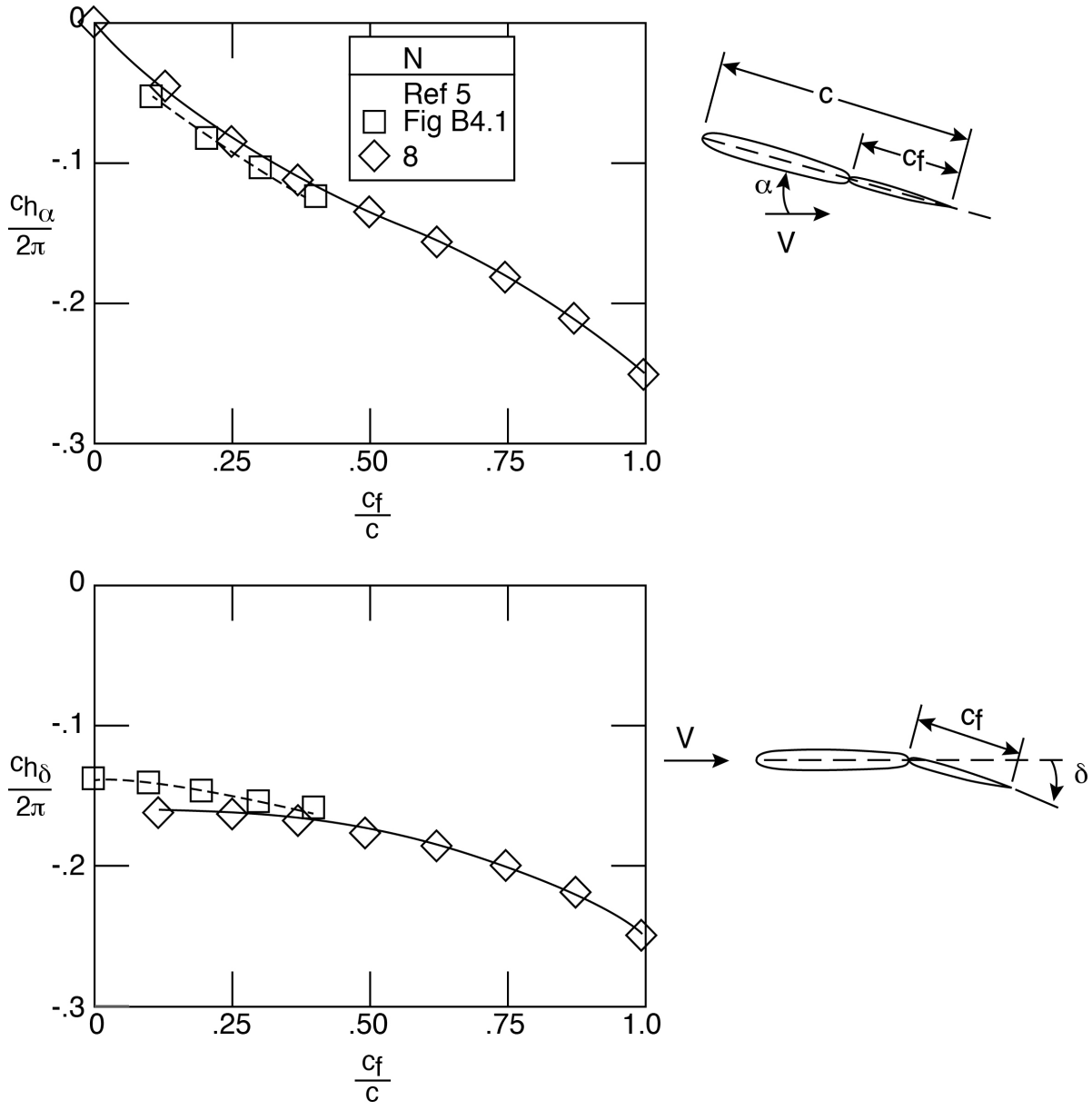

Figure 30. Steady state flap hinge-moment derivatives as a function of the ratio of flap chord to airfoil chord (plain flap with gap sealed)

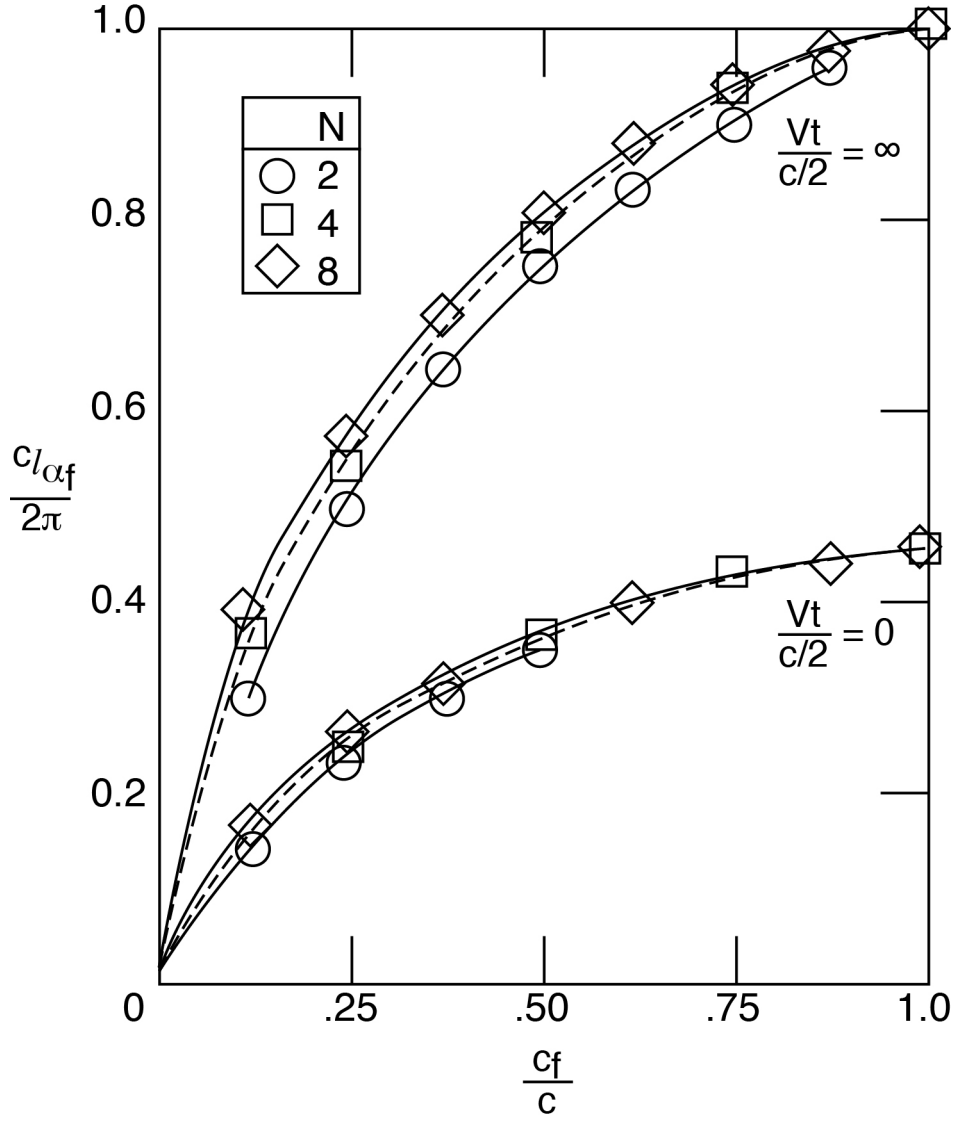

Figure 31. Lift derivative values due to a step input for the starting condition ($\frac{vt}{c/2} = 0$) and the terminal (steady-state) condition ($\frac{vt}{c/2} = \infty$) for flap attitude (i.e., flap angle of attack)

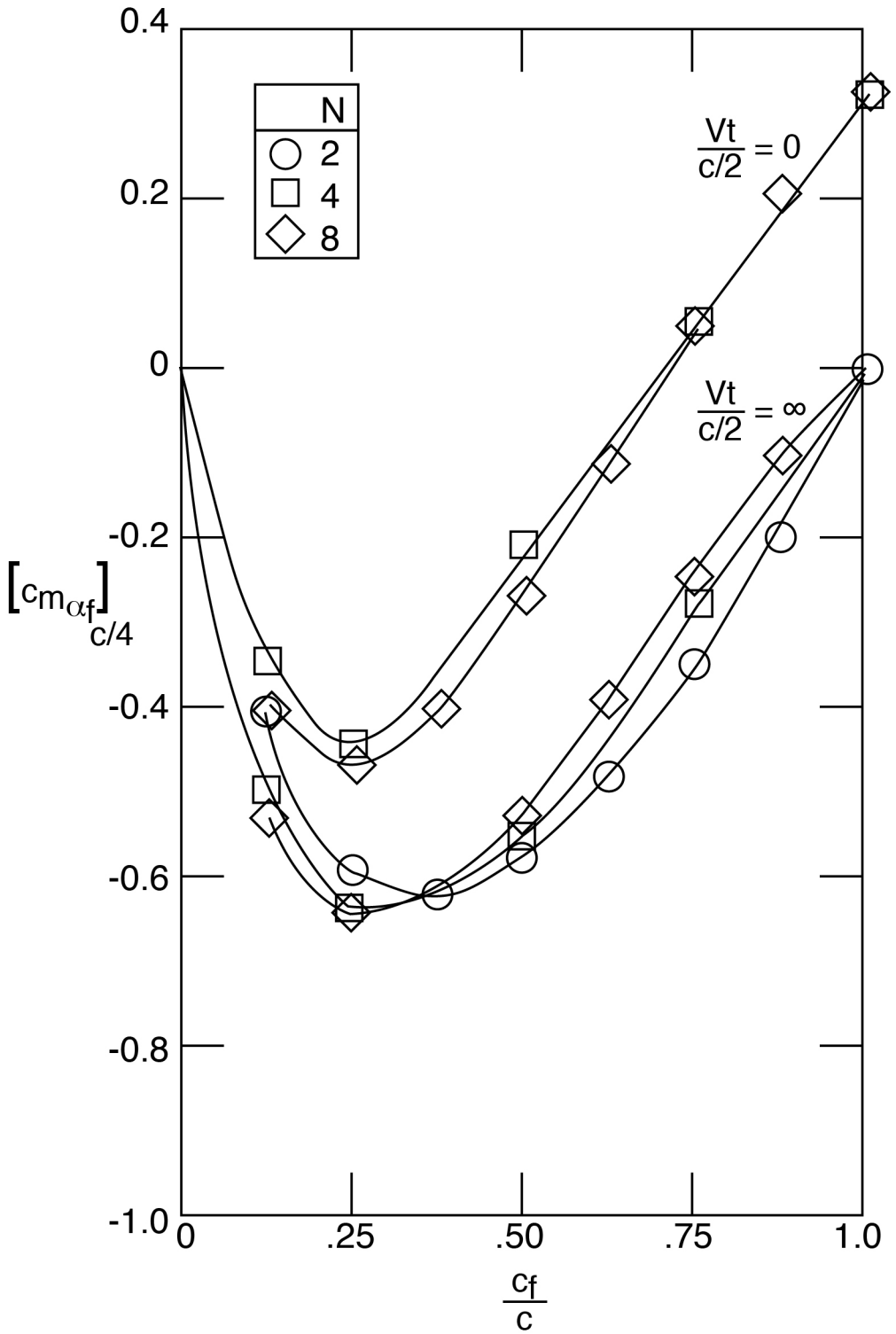

Figure 32. Moment derivative values due to a step input for the starting conditions ($\frac{vt}{c/2} = 0$) and the terminal (steady-state) condition ($\frac{vt}{c/2} = \infty$) for flap attitude (i.e., flap angle of attack)

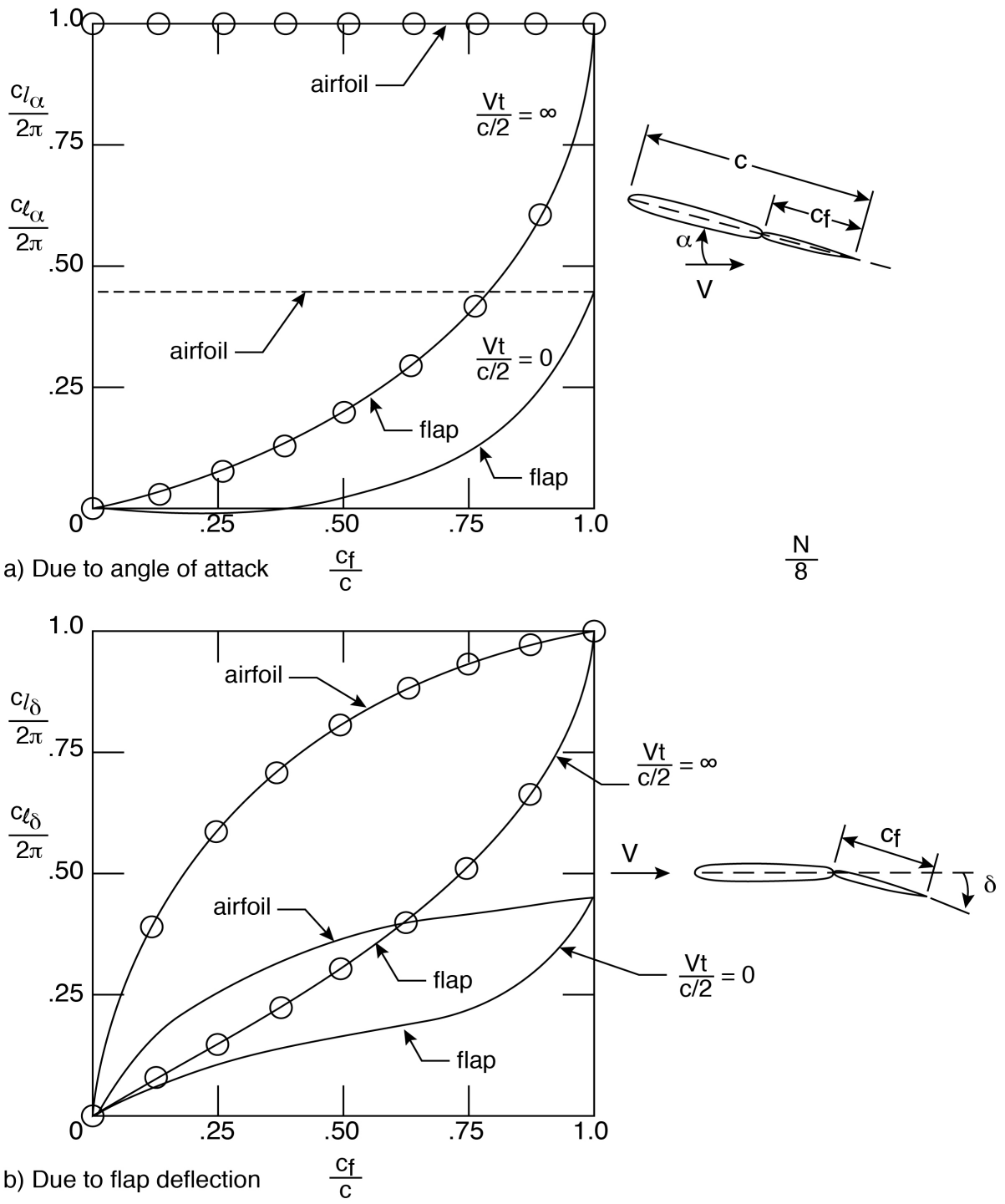

Figure 33. Flap lift to airfoil lift comparison for the steady-state ($\frac{vt}{c/2}=\infty$) and starting ($\frac{vt}{c/2}=0$) conditions

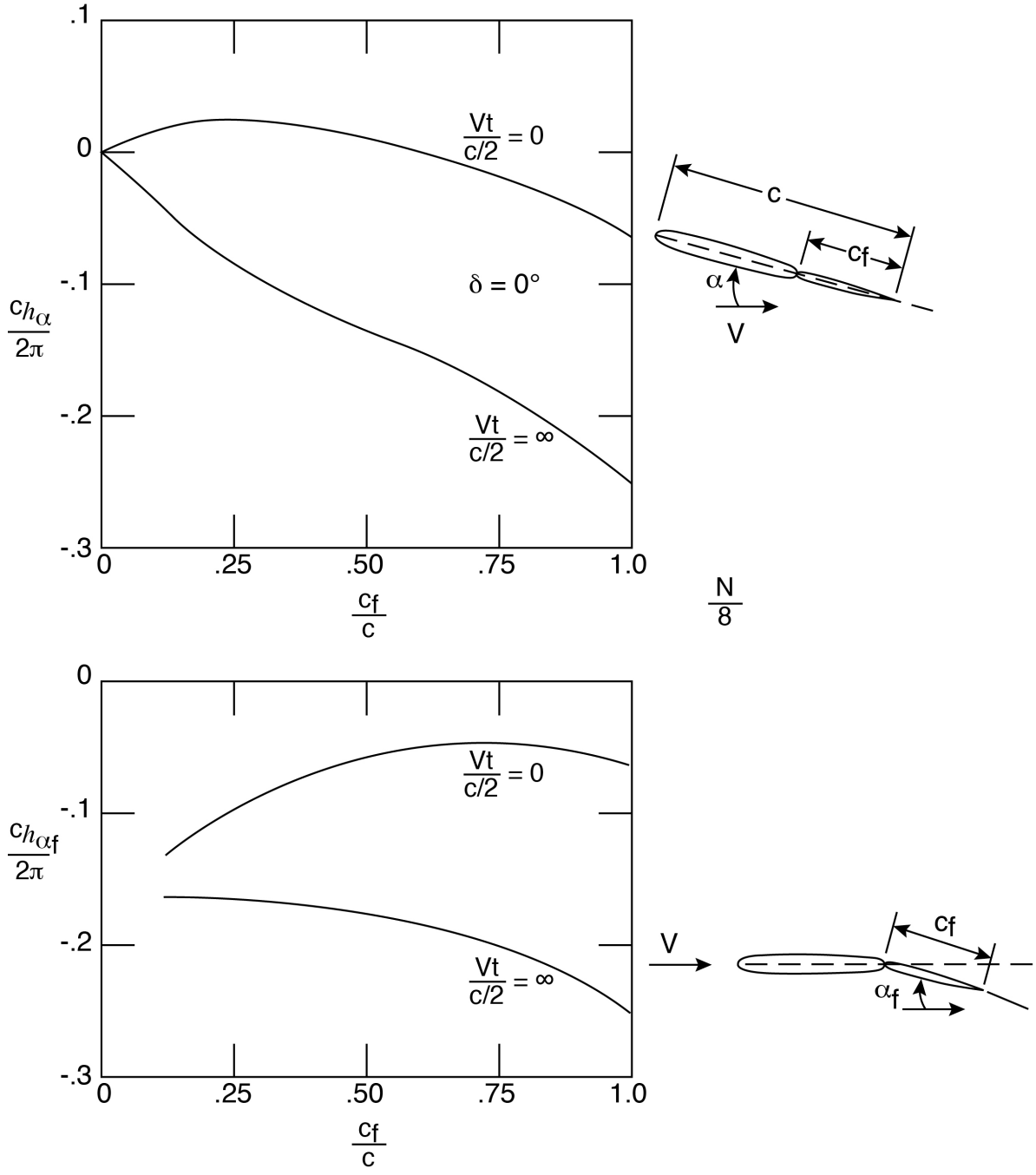

Figure 34. Flap hinge moment derivatives for the start ($\frac{vt}{c/2} = 0$) and termination ($\frac{vt}{c/2} = \infty$) conditions for step inputs in airfoil angle of attack and flap angle of attack

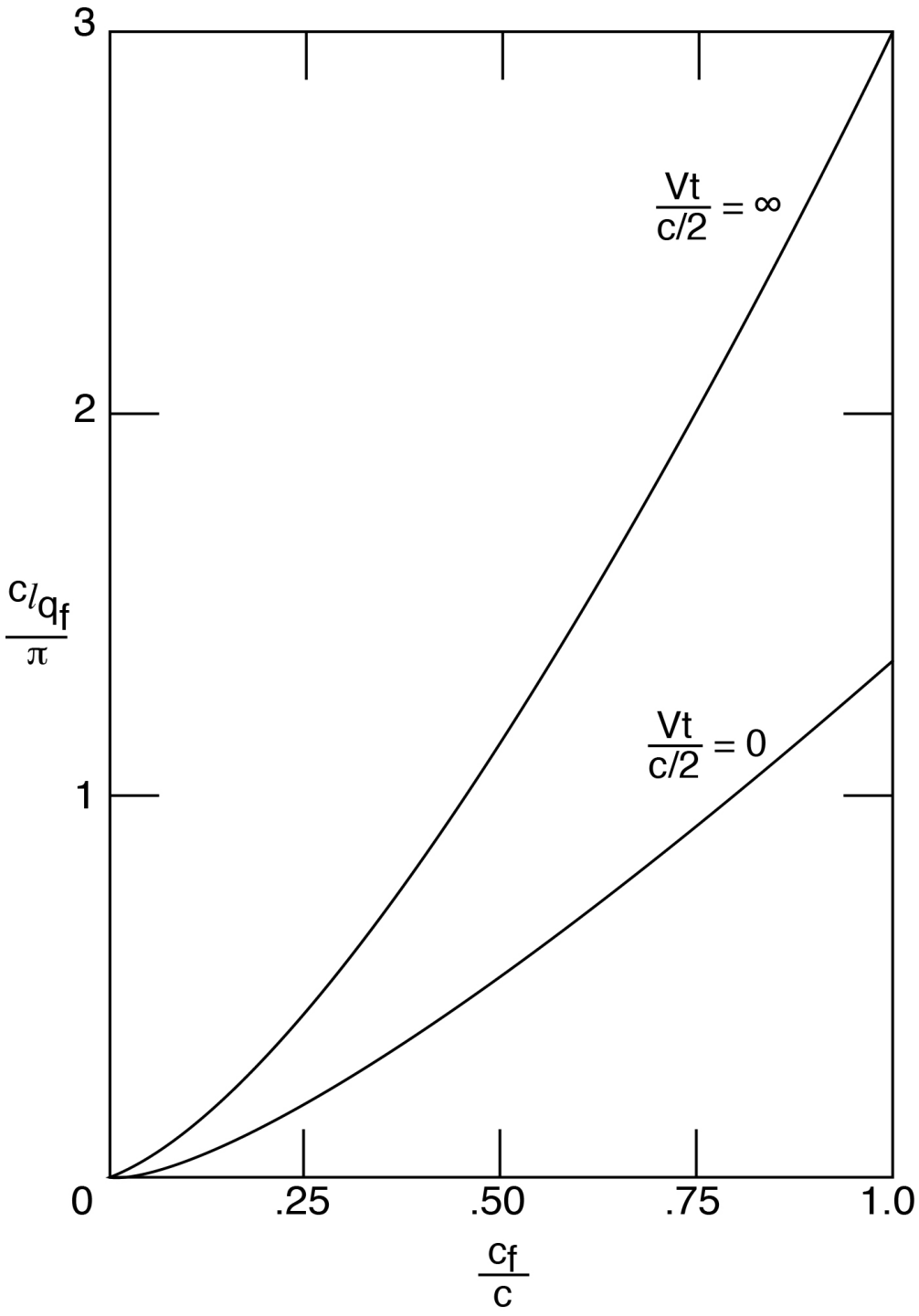

Figure 35. Lift derivative values due to a step input in flap angular velocity for starting ($\frac{vt}{c/2} = 0$) and termination ($\frac{vt}{c/2} = \infty$) conditions

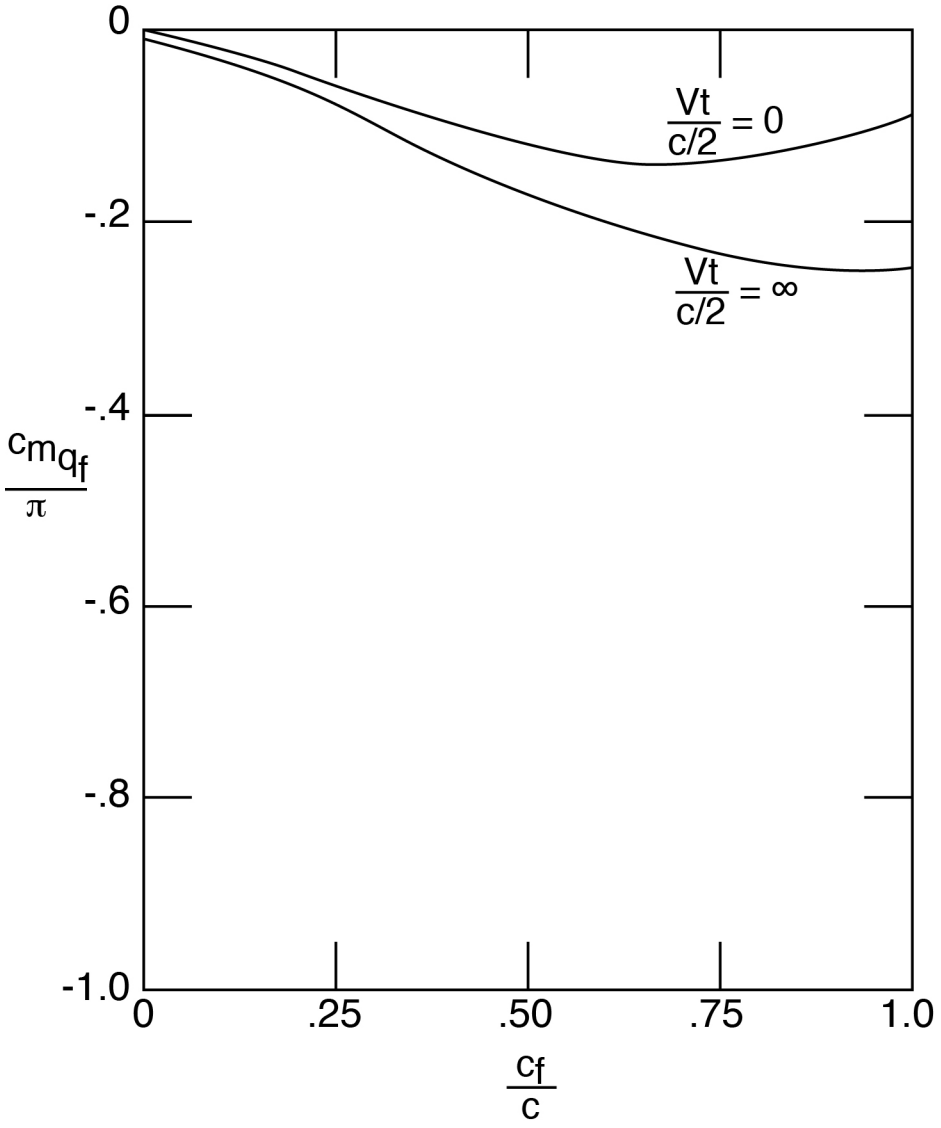

Figure 36. Moment derivative values due to a step input in flap angular velocity for starting ($\frac{vt}{c/2} = 0$) and termination ($\frac{vt}{c/2} = \infty$) conditions

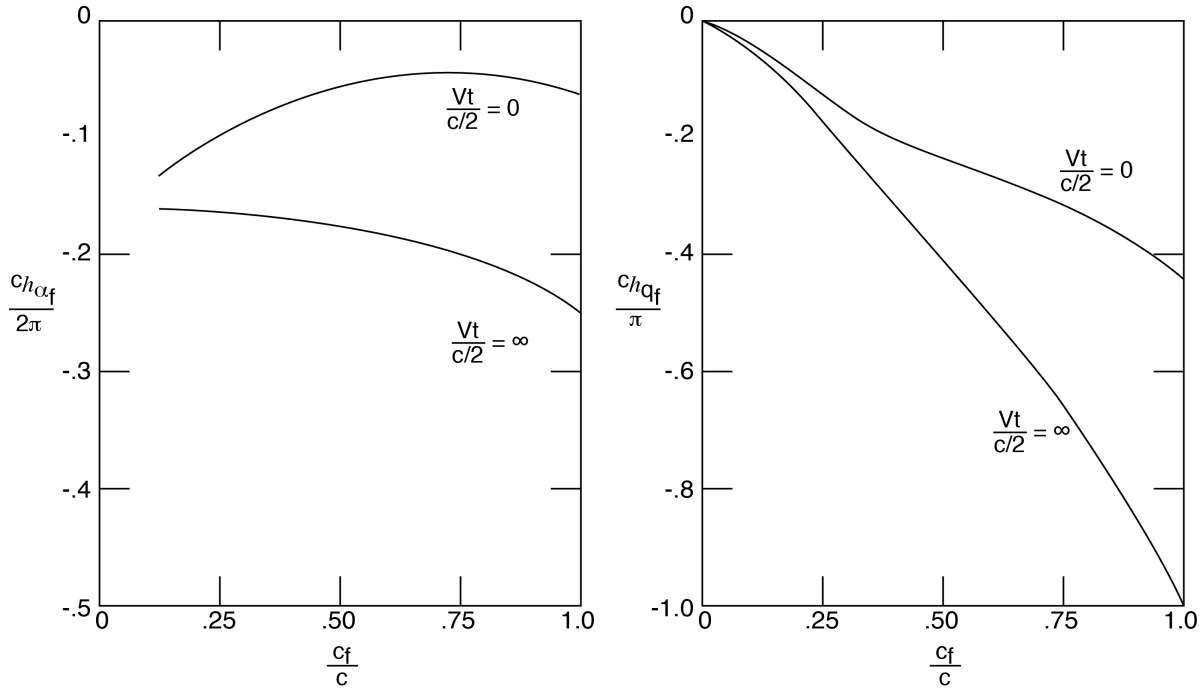

Figure 37. Values of flap hinge-moment derivatives for the start ($\frac{vt}{c/2} = 0$) and termination ($\frac{vt}{c/2} = \infty$) conditions for step inputs in flap angle of attack and flap pitch velocity

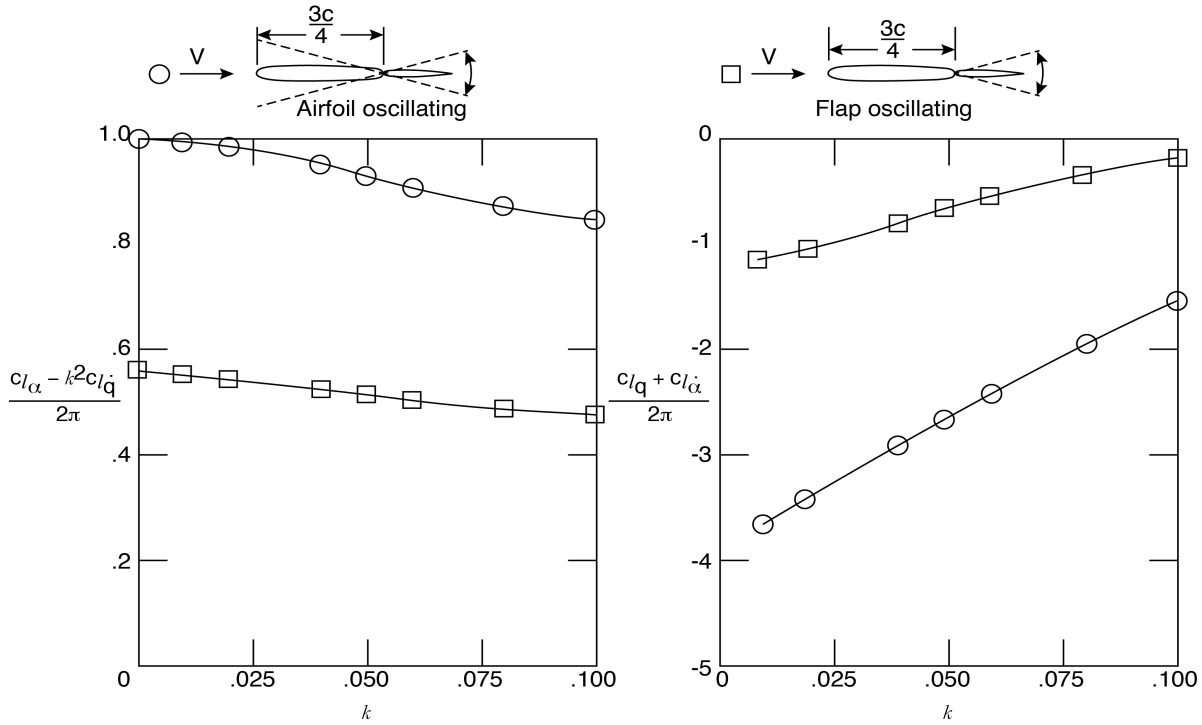

Figure 38. Comparison of airfoil lift derivatives with the airfoil oscillating and with only the quarter-chord flap oscillating

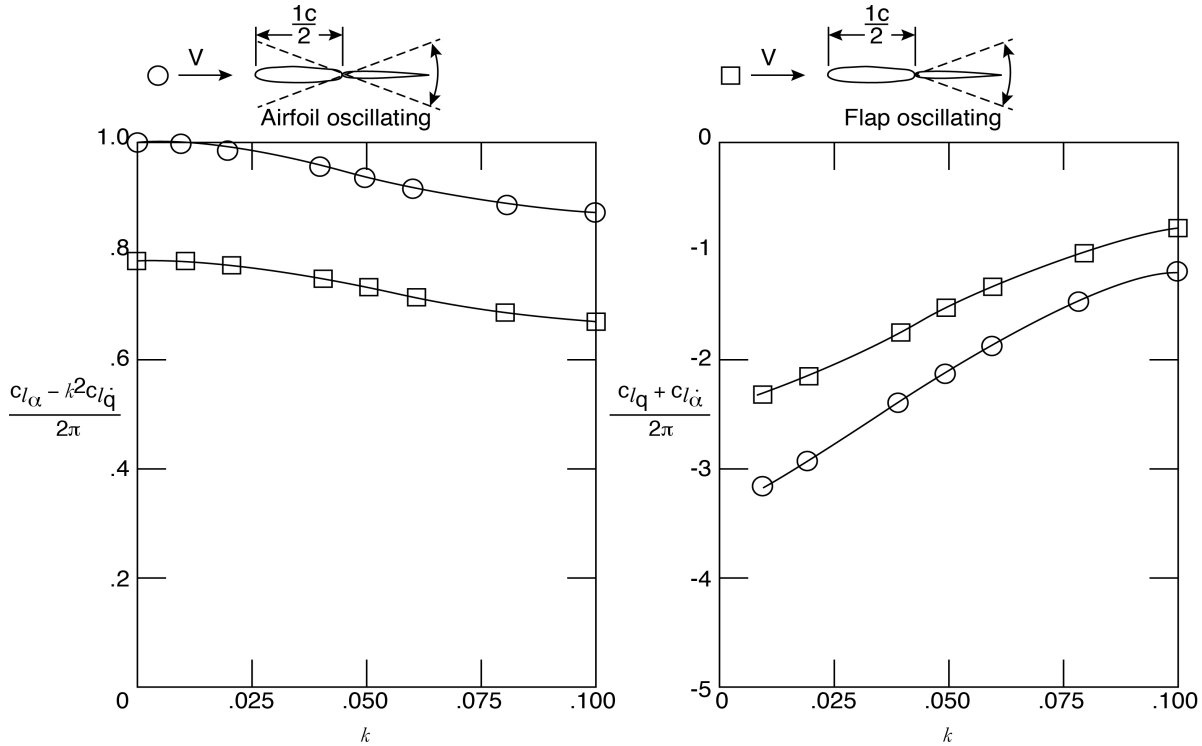

Figure 39. Comparison of airfoil lift derivatives with the airfoil oscillating and with only the half-chord flap oscillating

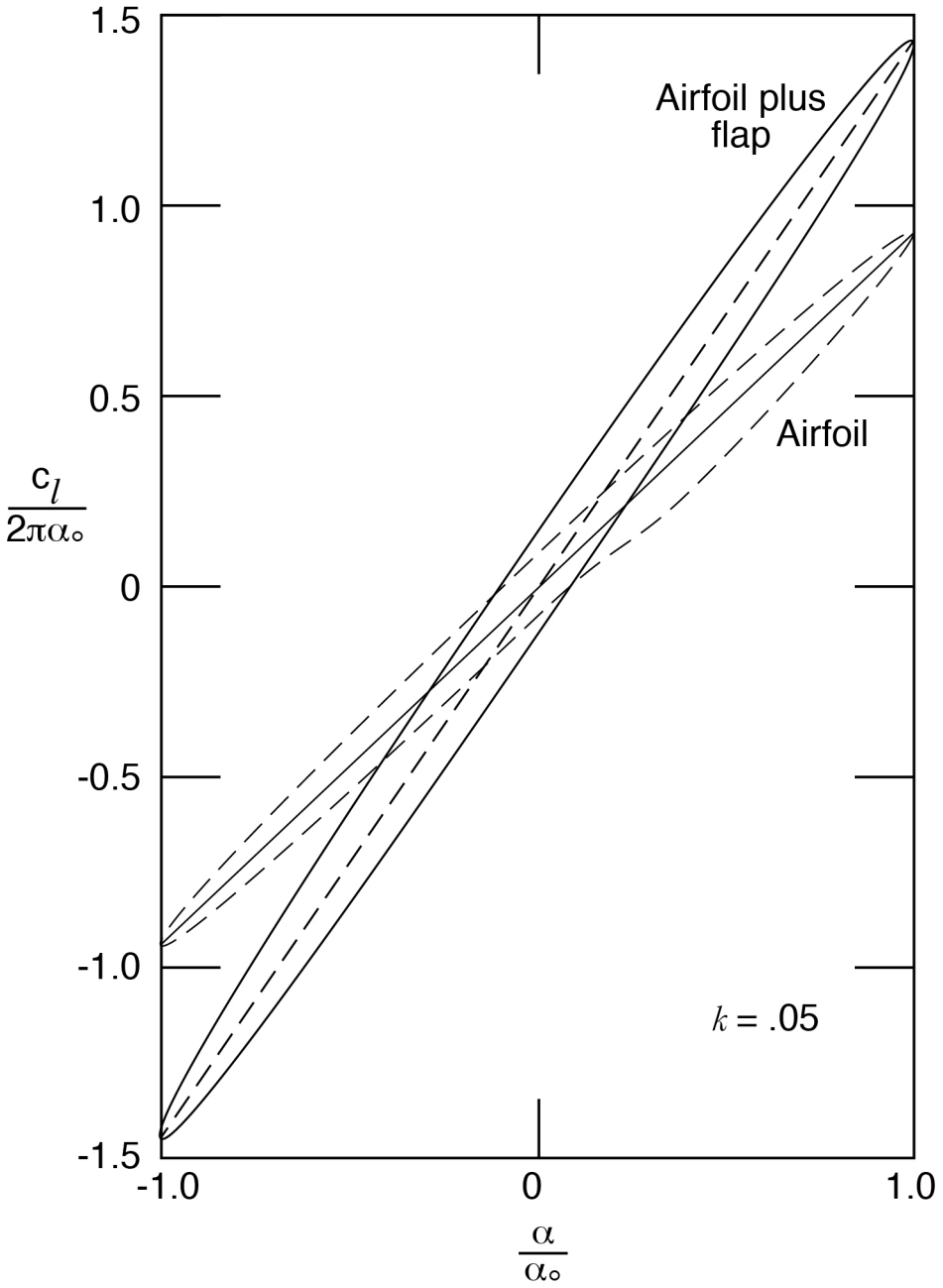

Figure 40. Lift-displacement trace for an airfoil oscillating about the mid-chord with flap undeflected and in combination with a quarter-chord flap oscillating with the same amplitude and frequency

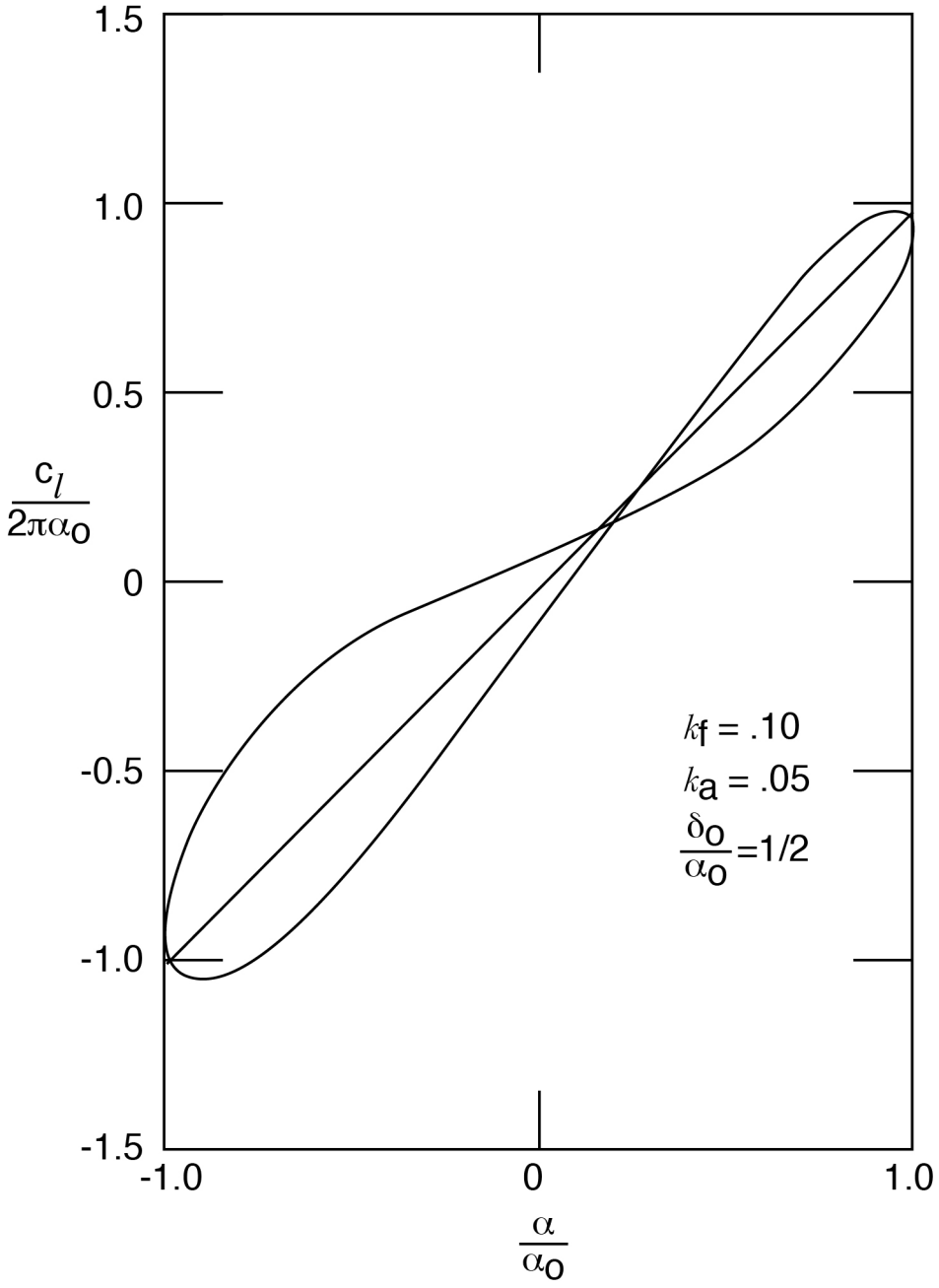

Figure 41. Lift-displacement trace for an airfoil oscillating about the mid-chord with a quarter-chord flap oscillating with one-half the amplitude and twice the frequency of the airfoil motion

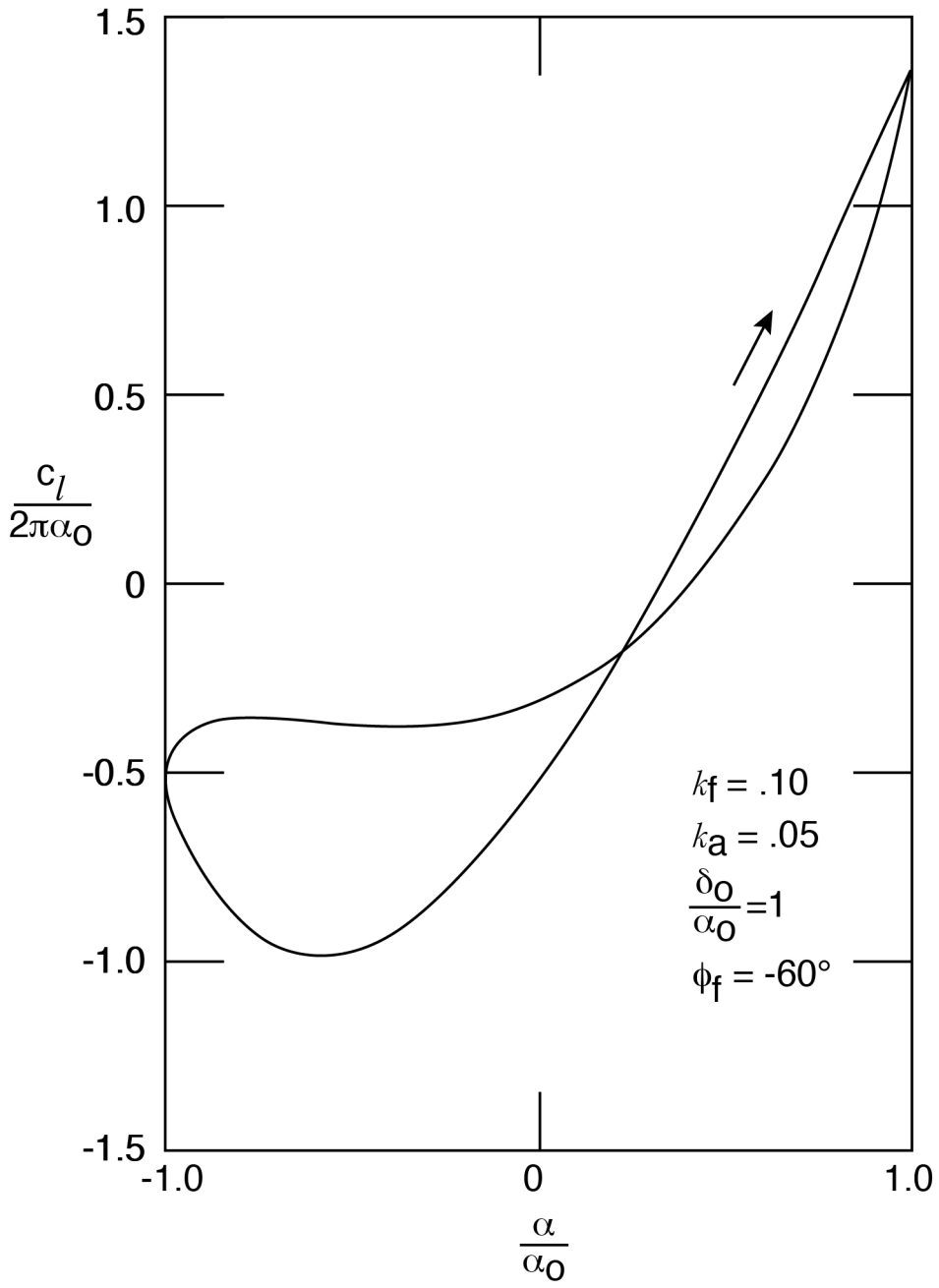

Figure 42. Lift-displacement trace for an airfoil oscillating about the mid-chord with a quarter-chord flap oscillating with the same amplitude and twice the frequency of the airfoil with $\phi_f = -60^o$

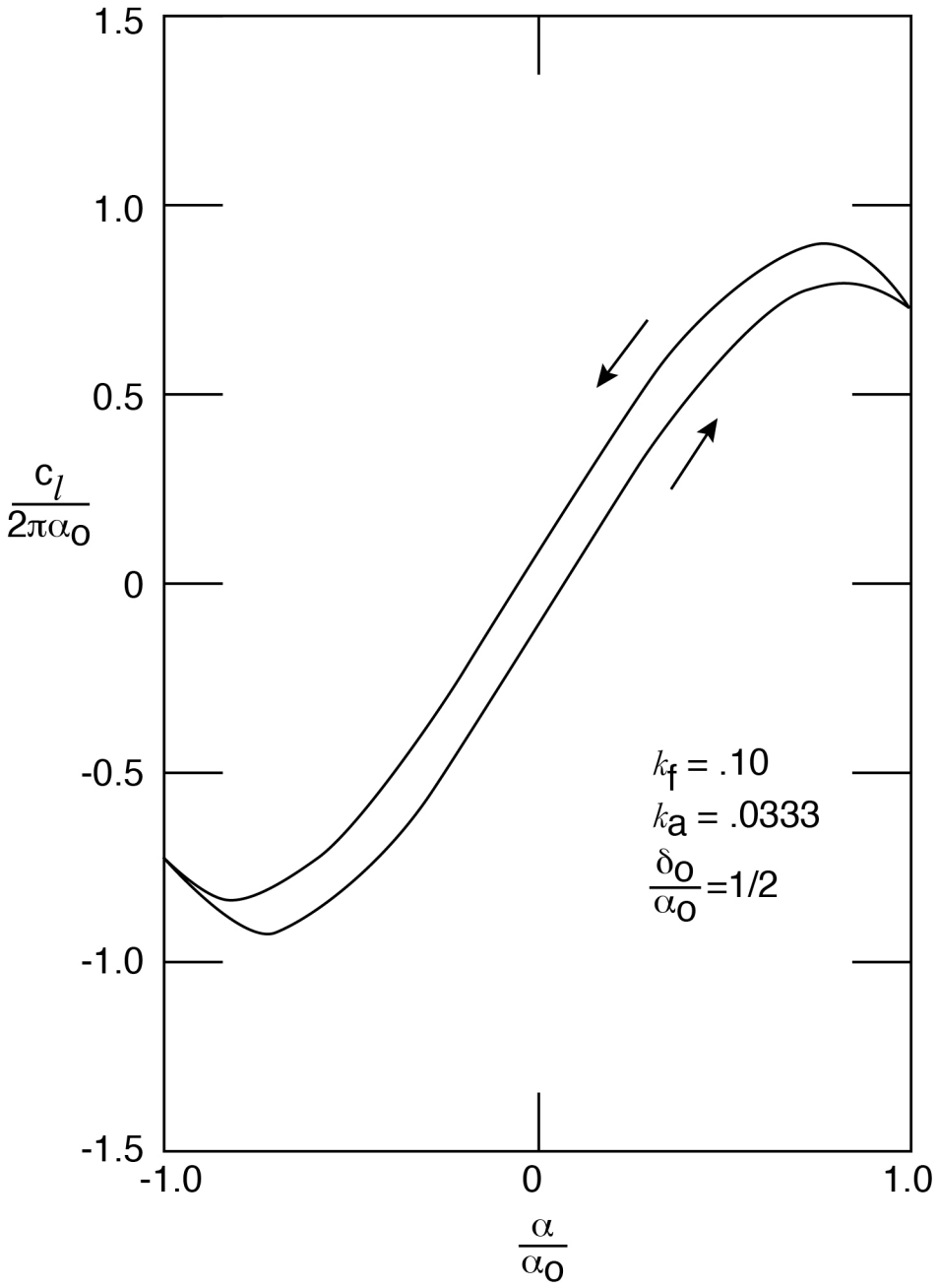

Figure 43. Lift-displacement trace for an airfoil oscillating about the mid-chord with a quarter-chord flap oscillating with half the amplitude and triple the frequency of the airfoil

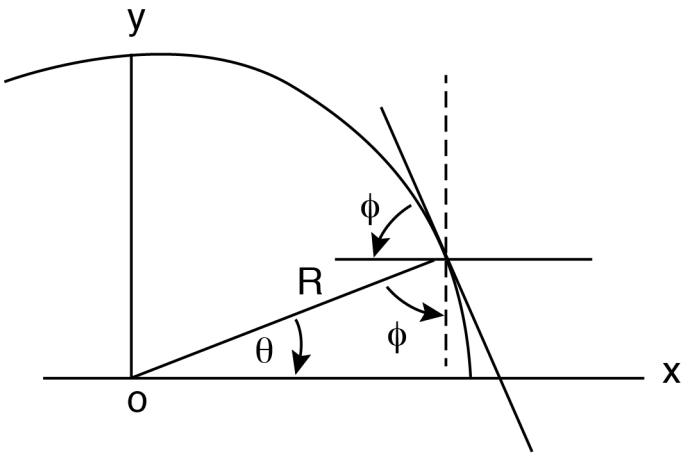

$$x^2 + y^2 = R^2$$

$$2xdx + 2ydy = 0$$

$$\frac{dy}{dx} = \frac{-x}{y} = \frac{-R\cos\theta}{R\sin\theta}$$

expressed in complementary angle ϕ

$$\frac{dy}{dx} = \frac{-\cos\theta}{\sin\theta} = \frac{-\sin\phi}{\cos\phi} = -\tan\phi$$

Figure 44a. Circular arc geometry

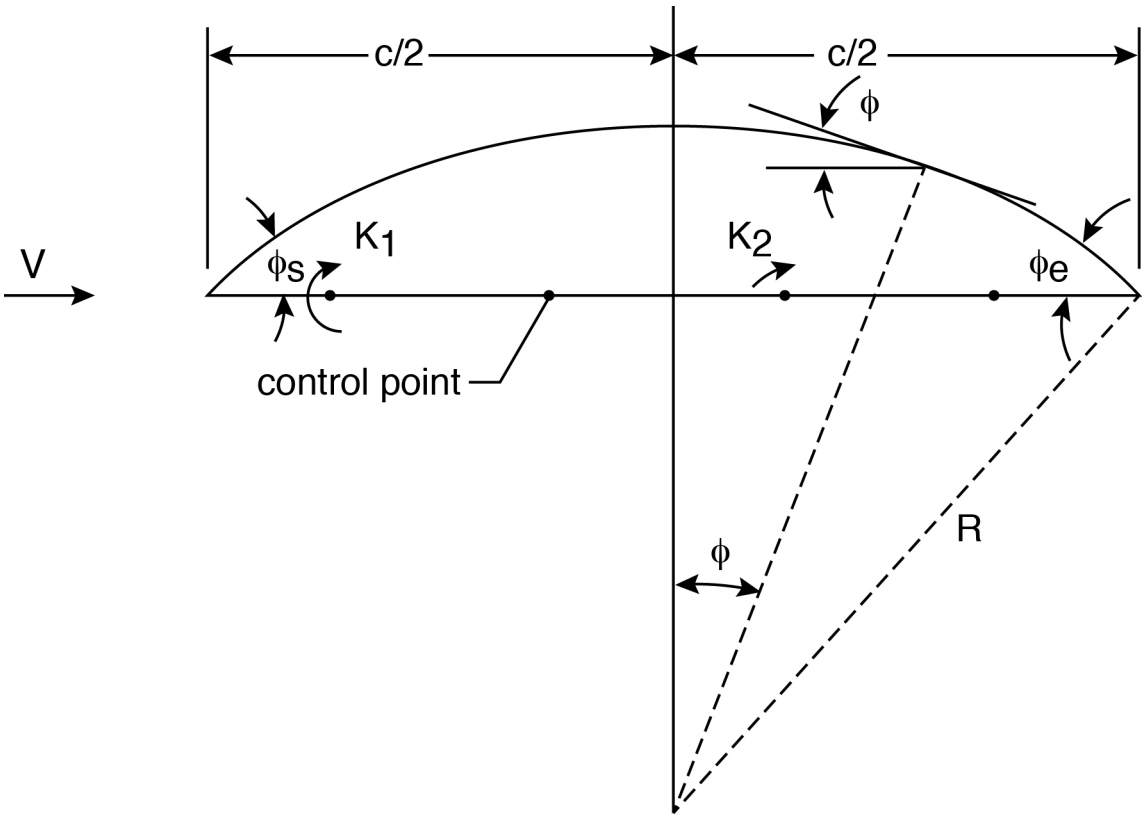

Sign change for curved surface for
wind from the left

$\frac{dy}{dx} = \tan \phi$

for small camber

$\frac{dy}{dx} = \phi$

external velocity normal to curved surface at any point = V sin ϕ

For small values of ϕ

$V \sin \phi = V\phi = \frac{\phi}{\phi_e} [\phi_e V]$

Figure 44b. Free stream flow normal component

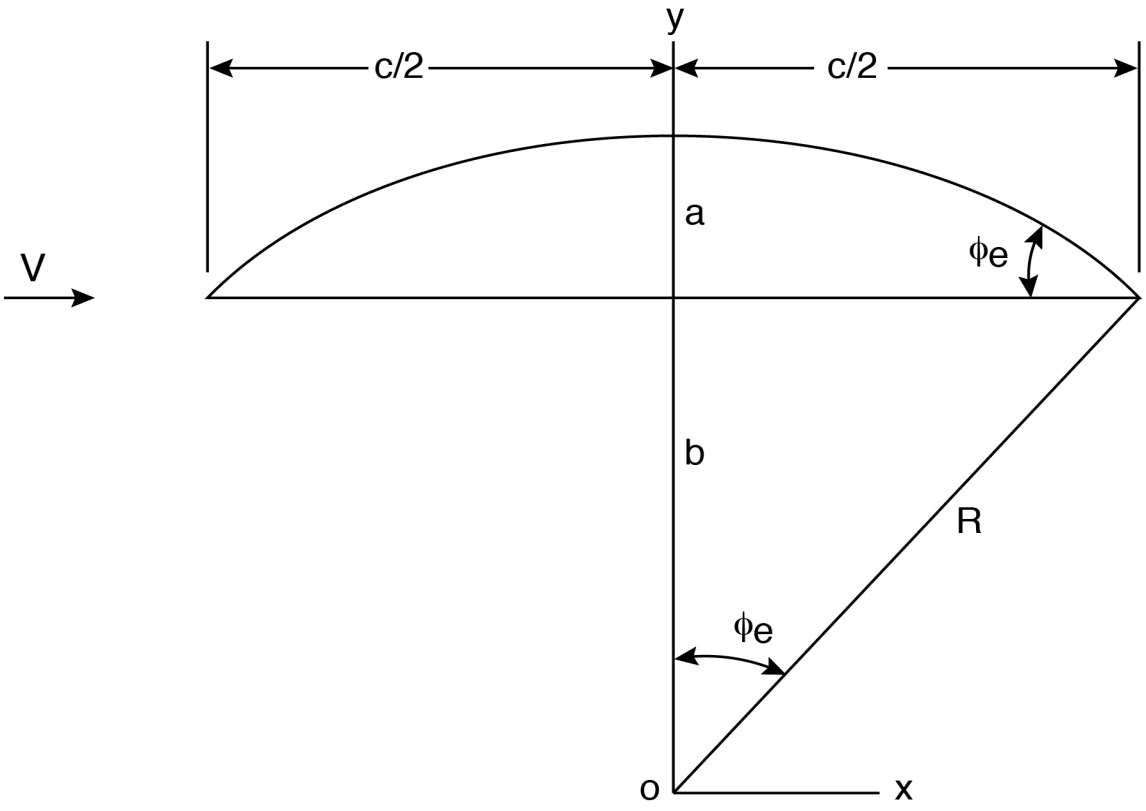

$$a = R - R\cos\phi_e$$

$$\frac{c}{2} = R\sin\phi_e$$

$$\frac{a}{c} = \frac{R\,[1-\cos\phi_e]}{2R\sin\phi_e}$$

Now $\cos\phi_e = 1 - \frac{\phi_e^2}{2!} + \frac{\phi_e^4}{4!}$ -----

For small ϕ_e, use 1st two terms

$$\frac{a}{c} = \frac{1-(1-\frac{\phi_e^2}{2!})}{2\phi_e} = \frac{\phi_e}{4}$$

Now camber parameter z is defined as $\frac{a}{c}$, thus

$$z = \frac{a}{c} = \frac{\phi_e}{4}$$

Figure 44c. Camber geometry

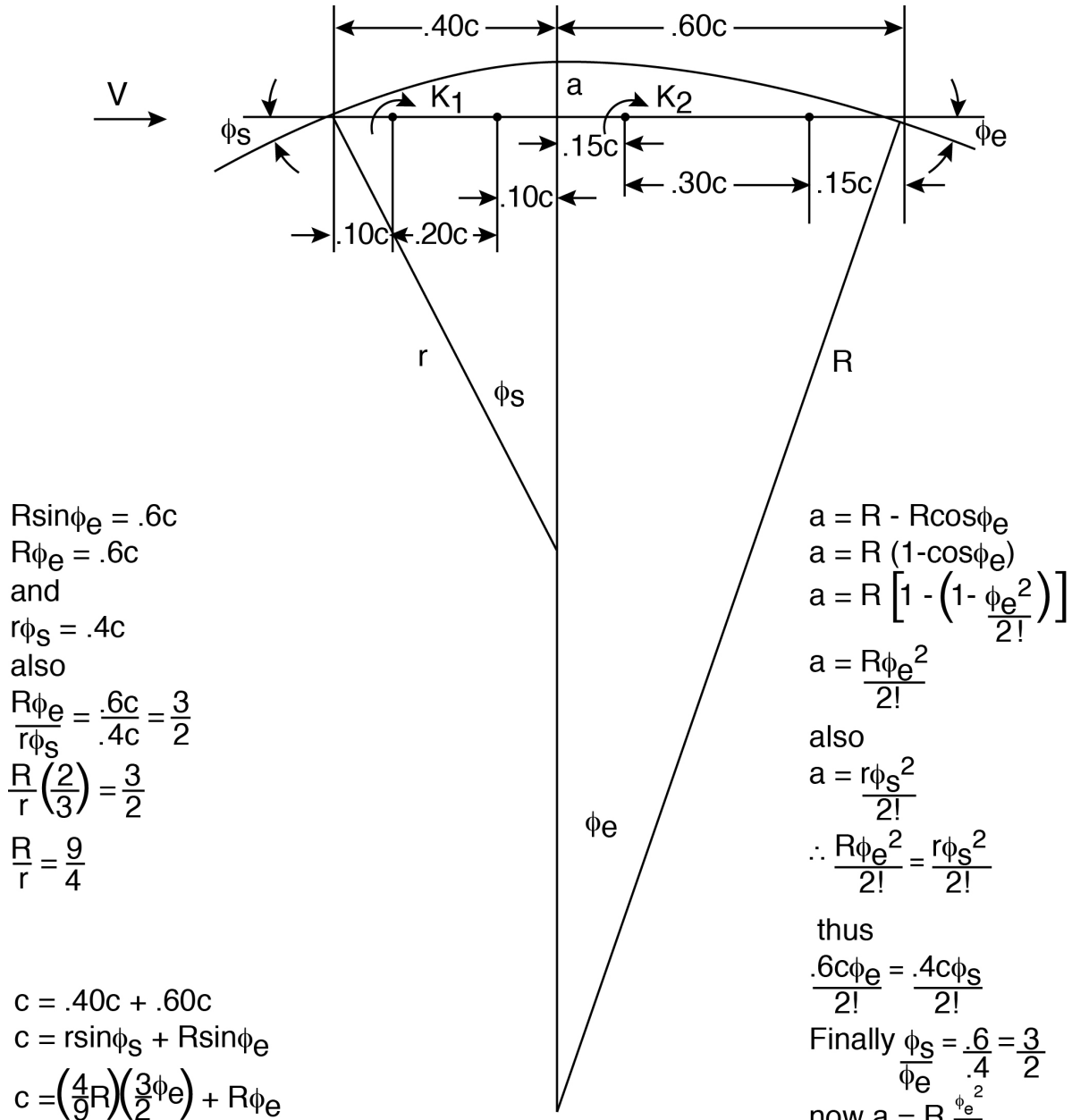

$R\sin\phi_e = .6c$

$R\phi_e = .6c$

and

$r\phi_s = .4c$

also

$$\frac{R\phi_e}{r\phi_s} = \frac{.6c}{.4c} = \frac{3}{2}$$

$$\frac{R}{r}\left(\frac{2}{3}\right) = \frac{3}{2}$$

$$\frac{R}{r} = \frac{9}{4}$$

$c = .40c + .60c$

$c = r\sin\phi_s + R\sin\phi_e$

$$c = \left(\frac{4}{9}R\right)\left(\frac{3}{2}\phi e\right) + R\phi_e$$

$$c = 1\frac{2}{3}R\phi_e = \frac{5}{3}R\phi_e$$

$a = R - R\cos\phi_e$

$a = R(1-\cos\phi_e)$

$$a = R\left[1 - \left(1 - \frac{\phi_e^2}{2!}\right)\right]$$

$$a = \frac{R\phi_e^2}{2!}$$

also

$$a = \frac{r\phi_s^2}{2!}$$

$$\therefore \frac{R\phi_e^2}{2!} = \frac{r\phi_s^2}{2!}$$

thus

$$\frac{.6c\phi_e}{2!} = \frac{.4c\phi_s}{2!}$$

Finally $\frac{\phi_s}{\phi_e} = \frac{.6}{.4} = \frac{3}{2}$

now $\frac{a}{c} = \frac{R\frac{\phi_e^2}{2!}}{\frac{5}{3}R\phi_e}$

$$z = \frac{a}{c} = \frac{3}{10}\phi_e$$

Figure 45. Geometry for two circular arcs (max camber at 0.4c)

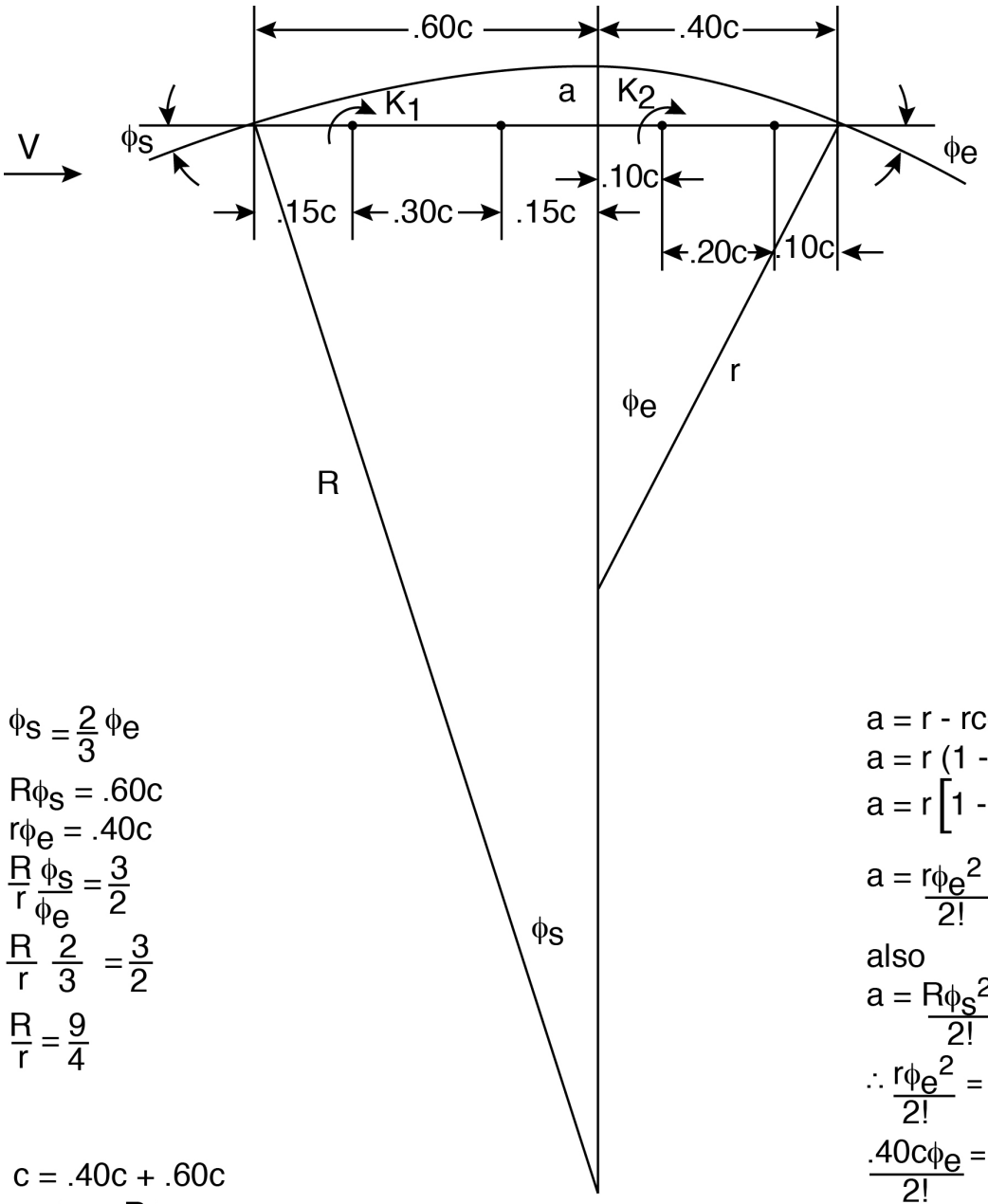

$\phi_s = \frac{2}{3}\phi_e$

$R\phi_s = .60c$

$r\phi_e = .40c$

$\frac{R}{r}\frac{\phi_s}{\phi_e} = \frac{3}{2}$

$\frac{R}{r}\ \frac{2}{3}\ = \frac{3}{2}$

$\frac{R}{r} = \frac{9}{4}$

$c = .40c + .60c$

$= r\phi_e + R\phi_s$

$= r\phi_e + \left(\frac{9}{4}r\right)\left(\frac{2}{3}\phi_e\right)$

$= r\phi_e\left(1\frac{3}{2}\right) = \frac{5}{2}r\phi_e$

$a = r - r\cos\phi_e$

$a = r\,(1 - \cos\phi_e)$

$a = r\left[1 - \left(1 - \frac{\phi_e^2}{2!}\right)\right]$

$a = \frac{r\phi_e^2}{2!}$

also

$a = \frac{R\phi_s^2}{2!}$

$\therefore \frac{r\phi_e^2}{2!} = \frac{R\phi_s^2}{2!}$

$\frac{.40c\phi_e}{2!} = \frac{.60c\phi_s}{2!}$

$\frac{\phi_s}{\phi_e} = \frac{.40}{.60} = \frac{2}{3}$

$\frac{a}{c} = \frac{r\frac{\phi_e^2}{2!}}{\frac{5}{2}r\phi_e}$

$z = \frac{a}{c} = \frac{2}{10}\phi_e = \frac{1}{5}\phi_e$

Figure 46. Geometry for two circular arcs (max camber at 0.6c)

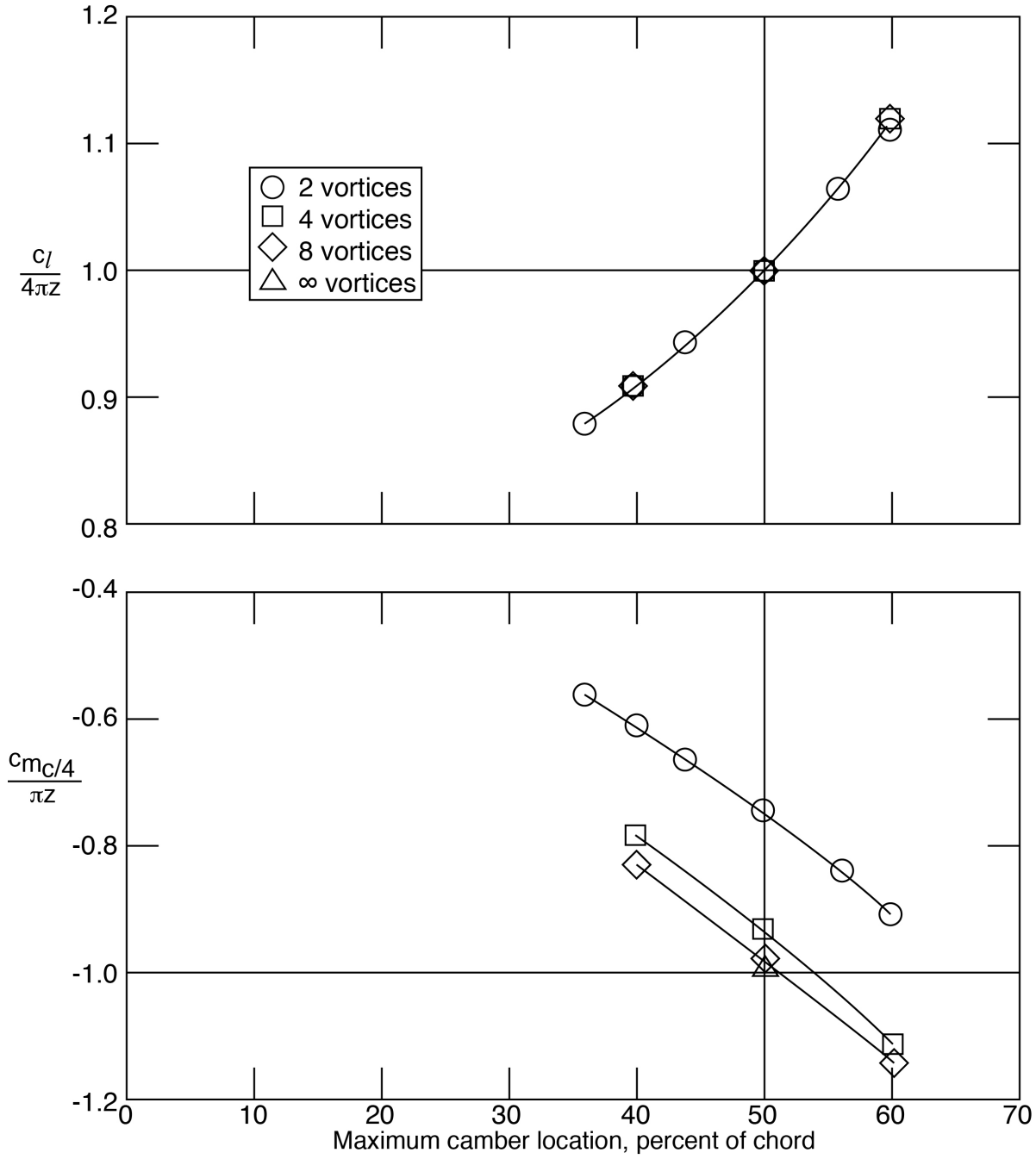

Figure 47. Lift and moment coefficients versus maximum camber location

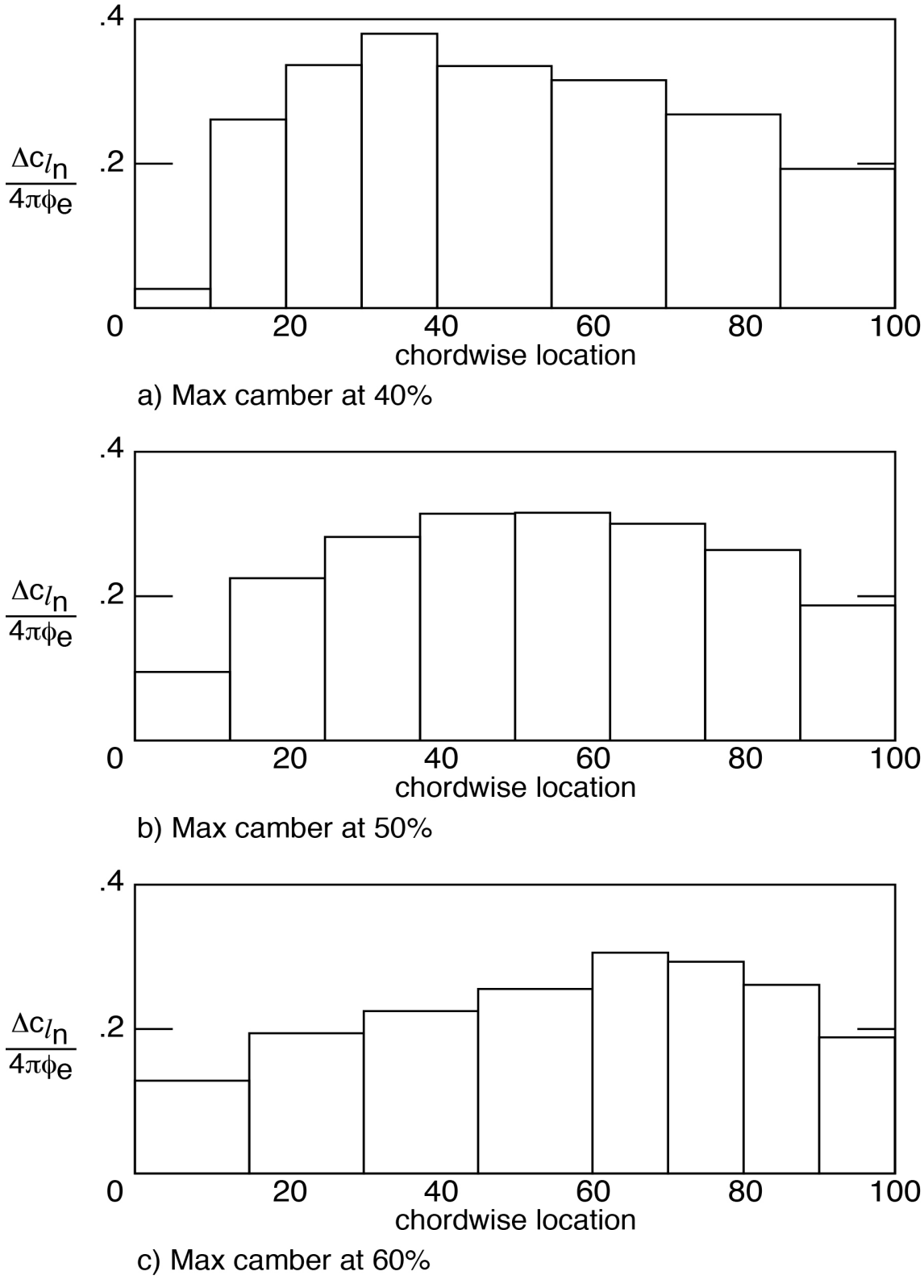

Figure 48. Chordwise load distribution for three maximum camber locations

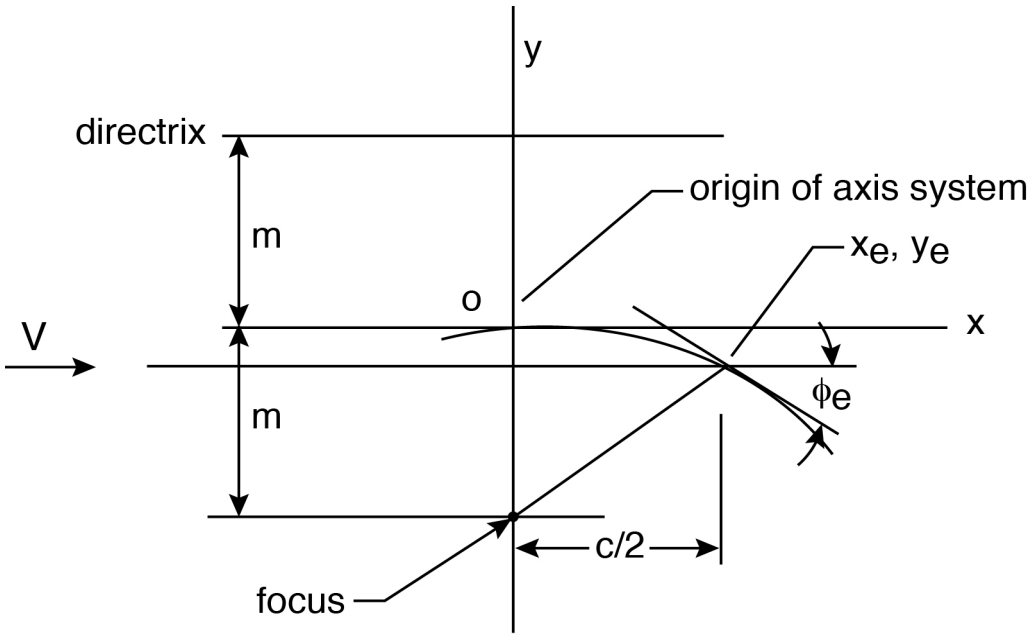

$x^2 = -4my$ ----------1

$2x\,dx = -4m\,dy$

$\frac{dy}{dx} = \frac{2x}{4m}$ ----------2

now from equation 1

$m = -\frac{x^2}{4Y}$

$\therefore \frac{dy}{dx} = \frac{2x}{4} \quad \frac{4y}{x^2} = \frac{2y}{x}$ ----------3

when $x = c/2$ $y = -y_e$ (the end point of meanline)

$\frac{dy}{dx} = \frac{2\,y_e}{c/2} = \frac{4\,y_e}{c}$

since $\frac{y_e}{c} = Z$ and $\frac{dy}{dx} = \text{fan}\,\phi_e = \phi_e$

$4Z = \phi_e$ ----------4

using equation 2, for any point x

$\frac{\phi}{\phi_e} = \frac{2x}{4m} \quad \frac{4m}{2x_e} = \frac{x}{x_e}$

and $\phi = \frac{x}{x_e}\phi_e$ ----------5

Figure 49. Camber geometry for NACA 4-digit series with max camber at 50% chord

REPORT DOCUMENTATION PAGE

Form Approved
OMB No. 0704-0188

1. REPORT DATE *(DD-MM-YYYY)*	2. REPORT TYPE	3. DATES COVERED *(From - To)*
01- 12 - 2015	Technical Memorandum	

4. TITLE AND SUBTITLE

Calculated Low-Speed Steady and Time-Dependent Aerodynamic Derivatives for Some Airfoils Using a Discrete Vortex Method

5a. CONTRACT NUMBER

5b. GRANT NUMBER

5c. PROGRAM ELEMENT NUMBER

6. AUTHOR(S)

Riley, Donald R.

5d. PROJECT NUMBER

5e. TASK NUMBER

5f. WORK UNIT NUMBER

432938.11.01.07.43.40.17

7. PERFORMING ORGANIZATION NAME(S) AND ADDRESS(ES)

NASA Langley Research Center
Hampton, VA 23681-2199

8. PERFORMING ORGANIZATION REPORT NUMBER

L-20616

9. SPONSORING/MONITORING AGENCY NAME(S) AND ADDRESS(ES)

National Aeronautics and Space Administration
Washington, DC 20546-0001

10. SPONSOR/MONITOR'S ACRONYM(S)

NASA

11. SPONSOR/MONITOR'S REPORT NUMBER(S)

NASA-TM-2015-218998

12. DISTRIBUTION/AVAILABILITY STATEMENT

Unclassified - Unlimited
Subject Category 34
Availability: NASA STI Program (757) 864-9658

13. SUPPLEMENTARY NOTES

14. ABSTRACT

This paper contains a collection of some results of four individual studies presenting calculated numerical values for airfoil aerodynamic stability derivatives in unseparated inviscid incompressible flow due separately to angle-of-attack, pitch rate, flap deflection, and airfoil camber using a discrete vortex method. Both steady conditions and oscillatory motion were considered. Variables include the number of vortices representing the airfoil, the pitch axis / moment center chordwise location, flap chord to airfoil chord ratio, and circular or parabolic arc camber. Comparisons with some experimental and other theoretical information are included. The calculated aerodynamic numerical results obtained using a limited number of vortices provided in each study compared favorably with thin airfoil theory predictions. Of particular interest are those aerodynamic results calculated herein (such as induced drag) that are not readily available elsewhere.

15. SUBJECT TERMS

Aerodynamic; Airfoils; Calculated; Derivatives; Discreet; Low-Speed; Method; Steady; Time-Dependent; Vortex

16. SECURITY CLASSIFICATION OF:			17. LIMITATION OF ABSTRACT	18. NUMBER OF PAGES	19a. NAME OF RESPONSIBLE PERSON
a. REPORT	b. ABSTRACT	c. THIS PAGE			STI Help Desk (email: help@sti.nasa.gov)
					19b. TELEPHONE NUMBER *(Include area code)*
U	U	U	UU	66	(757) 864-9658